BLAST WAVE FROM A HIGH-PRESSURE GAS TANK RUPTURE IN A FIRE: STAND-ALONE AND UNDER-VEHICLE HYDROGEN TANKS

Molkov, V., Kashkarov, S.

Hydrogen Safety Engineering and Research Centre (HySAFER), University of Ulster, Newtownabbey, BT37 0QB, Northern Ireland, UK
v.molkov@ulster.ac.uk, kashkarov-s@email.ulster.ac.uk

ABSTRACT

This study addresses one of knowledge gaps in hydrogen safety science and engineering, i.e. a predictive model for calculation of deterministic separation distances defined by the parameters of a blast wave generated by a high-pressure gas storage tank rupture in a fire. An overview of existing methods to calculate stored in a tank internal (mechanical) energy and a blast wave decay is presented. Predictions by the existing technique and an original model developed in this study, which accounts for the real gas effects and combustion of the flammable gas released into the air (chemical energy), are compared against experimental data on high-pressure hydrogen tank rupture in the bonfire test. The main reason for a poor predictive capability of the existing models is the absence of combustion contribution to the blast wave strength. The developed methodology is able to reproduce experimental data on a blast wave decay after rupture of a stand-alone hydrogen tank and a tank under a vehicle. In this study, the chemical energy is dynamically added to the mechanical energy and is accounted for in the energy-scaled non-dimensional distance. The fraction of the total chemical energy of combustion released to feed the blast wave is 5% and 9%, however it is 1.4 and 30 times larger than the mechanical energy in the stand-alone tank test and the under-vehicle tank test respectively. The model is applied as a safety engineering tool to four typical hydrogen storage applications, including on-board vehicle storage tanks and a stand-alone refuelling station storage tank. Harm criteria to people and damage criteria for buildings from a blast wave are selected by the authors from literature to demonstrate the calculation of deterministic separation distances. Safety strategies should exclude effects of fire on stationary storage vessels, and require thermal protection of on-board storage to prevent dangerous consequences of high-pressure tank rupture in a fire.

KEYWORDS: blast wave, overpressure, impulse, fire, deterministic separation distance, hydrogen, model, mechanical and chemical energy.

NOMENCLATURE

a_g	speed of sound in compressed gas (m/s)
a_s	speed of sound in surrounding gas (m/s)
B	batch availability (J)
b	co-volume constant, b=1.584×10^{-5} m^3/mol, or b=7.69×10^{-3} m^3/kg
c_v	specific heat at constant volume (J/kg/K)
c_p	specific heat at constant pressure (J/kg/K)
E_{ch}	total chemical energy (J)
E_m	total mechanical energy (J)
E_i	combustion products expansion coefficient of stoichiometric hydrogen-air mixture
H	enthalpy (J)
H_c	heat of combustion (J/kg)
I	impulse (Pa·s)
$\bar{I}$	non-dimensional impulse
L_{SUV}	length of SUV (m)
M	molecular mass, kg/mol
M_{sh}	Mach number of the shock wave
m	mass (kg)
m_g	mass of compressed gas (kg)
n	number of gas moles (mol)
ΔP	overpressure in a blast wave (Pa)
$\bar{P}_{st}$	non-dimensional starting shock overpressure
$\bar{P}$	non-dimensional overpressure, $\bar{P}=P/p_s$
p	pressure (Pa)
p_f	pressure at final stage of gas expansion (Pa)
p_g	pressure of gas in a vessel (Pa)
p_i	pressure of gas at initial state (Pa)
p_s	surrounding pressure, Pa

R	universal gas constant, R=8.314 J/mol/K
r	distance from a vessel (m)
r_b	radius of hemisphere occupied by combustion products of burned stoichiometric hydrogen-air mixture (m)
r_{sh}	radius of shock wave (m)
r_u	radius of hemisphere occupied by unburned hydrogen-air mixture (m)
r_v	radius of spherical vessel of equivalent volume (m)
$\bar{r}$	non-dimensional distance from a vessel (non-dimensionalised for overpressure)
$\bar{r}_I$	non-dimensional distance from a vessel for impulse calculation
$\bar{r}_P$	non-dimensional distance from a vessel for overpressure calculation
$\bar{r}_v$	non-dimensional energy-scaled radius of spherical vessel
S	entropy (J/K)
T	temperature (K)
T_f	gas temperature at final stage of expansion (K)
T_i	initial temperature of compressed gas (K)
T_s	surrounding temperature (K)
V	volume (m^3)
V_b	volume of hemisphere occupied by combustion products of burned stoichiometric hydrogen-air mixture (m^3)
V_f	volume of expanded gas (m^3)
V_i	initial volume of compressed gas, i.e. vessel volume (m^3)
V_{sh}	volume of hemisphere behind a shock (m^3)
V_u	volume of a hemisphere occupied by stoichiometric hydrogen-air mixture (m^3)
W	total work performed by gas (J)
W_{SUV}	width of SUV (m)

Greek

α	mechanical energy coefficient
β	chemical energy coefficient
γ	ratio of specific heats
π	"pi" number
ρ	density (kg/m^3)
φ	"steady flow" availability (J)

Subscripts

a	air
b	burned
ch	chemical
f	final
g	gas
I	impulse
i	initial
m	mechanical
P	overpressure
s	surrounding
sh	shock
st	starting shock
SUV	sport utility vehicle
u	unburned
v	vessel

Abbreviations

CFRP	carbon fibre reinforced polymer
CNG	Compressed Natural Gas
HRR	heat release rate
IR	infrared
LPG	liquefied petroleum gas
OEM	Original Equipment Manufacturer
SUV	sport utility vehicle
TPRD	thermally activated pressure relief device

1.0 INTRODUCTION

The use of alternative fuels like compressed natural gas (CNG), liquefied petroleum gas (LPG), and hydrogen raises the safety issues that have to be addressed. One of these issues is a blast wave strength that is needed to calculate a deterministic separation distance when high-pressure storage tank ruptures in a fire. Hydrogen safety engineering is a new discipline underpinning the technological safety of emerging hydrogen systems and infrastructure. It encompasses previously acquired and recent knowledge generated by the international hydrogen safety community that is published elsewhere [1]. The separation distance is an ultimate mitigation measure against hazards and associated risks during an accident that involves, in particular, compressed hydrogen storage. One of technical features that makes hydrogen systems different from others is very high storage pressure up to 100 MPa.

Deterministic separation distance from a hydrogen system or infrastructure is usually assessed by either hazards of unignited or ignited (fire) release from equipment or storage, or by hazards

associated with a catastrophic failure (rupture) of a storage vessel, particularly in a fire. In the last case a strong blast wave is followed by a comparatively large size fireball. In the case of unignited non-catastrophic release, e.g. from failed thermally activated pressure release device (TPRD), the deterministic separation distance should exclude, for example, an intake of a flammable mixture into a building to prevent an explosion. This means that a deterministic separation distance should be longer than a size of the flammable envelope (distance from a release source to the lower flammability limit, i.e. concentration of 4% by volume of hydrogen in air). In the case of jet fire the "no harm" distance is 3.5 times longer than the flame length if the buoyancy effect is not accounted for [2] [2] . It has been demonstrated that all three separation distances for a jet fire, i.e. "no-harm", "pain" and "fatality", are equal or longer than a size of the flammable envelope for unignited release from the same leak source [2]. Thus, for non-catastrophic release in the form of a jet, in many cases a hydrogen safety engineer could limit him/herself by the calculation of deterministic separation distances from a jet fire only.

However, for a catastrophic release in the case of high-pressure tank rupture the situation is different. There are harmful phenomena like pressure effects from a blast wave and thermal effects from a fireball that are not yet studied for hydrogen to produce contemporary models and engineering tools for the hazard assessment.

The probability of a catastrophic failure of a high-pressure vessel is still a topic under discussion within the international safety community. One group of experts assumes that the probability of a catastrophic tank failure is so small that this scenario could be removed from the quantitative risk assessment at all. Authors of this paper belong to another group who thinks that the catastrophic tank failure, especially in fire conditions, must be a part of hazard and associated risk analysis. This is supported by a statistics on fractions of catastrophic failures of vessels and pipes gathered from established industries [3]. The historical incident databases and recommendations for risk analysis state that for vessels 73-90% of all releases are from the holes and about 10-27% releases are classified as a catastrophic failure (including storage tanks, LPG, oil, gas and chemical industries; covering the USA and European sources). The fraction of catastrophic failure for hydrogen tanks could be even higher as experiments show that if a high-pressure vessel/pipeline starts to leak through a "crack" then it immediately develops to catastrophic failure, i.e. full bore rupture of high pressure pipeline or full destruction of a vessel.

TPRDs are used to blow-down hydrogen from a storage tank in the case of fire "to prevent its catastrophic failure". Unfortunately, TPRD could be impossible to activate in some scenarios, e.g. in the case of a fire affecting only localized area of a tank far from TPRD, or when a car design allows to block TPRD sensing element by jammed parts of car(s) during a road accident without a chance to be initiated. Tank rupture in a fire is followed by a large fireball up to few tens of meters in diameter and its lifting above the ground by few seconds, as observed in experiments [4], and outwards propagating blast wave. These two hazards have to be considered when a safety engineer chooses a longest deterministic separation distance and estimates the risk.

In the case of catastrophic failure of an on-board high-pressure storage tank in a fire, the deterministic separation distance is a function of pressure effects of a blast wave, generated projectiles including a vehicle itself, and thermal effects that include direct engulfment by the high temperature fire products and harmful thermal radiation from a fireball up to some distance.

Deterministic separation distances for free unignited and ignited (fire) jet releases is now well understood and respective engineering tools are developed. Contrary to this, techniques to calculate separation from blast wave and fireball after high-pressure hydrogen storage tank rupture in a fire are absent.

There are a number of open questions in hydrogen safety science and engineering, which are not yet resolved. One of these questions, which will be addressed in this study, is whether hydrogen combustion, after a high-pressure tank rupture in a fire, contributes into the blast wave strength or not. Currently, there is a widespread opinion that combustion does not contribute to the blast wave strength. This opinion is based on the assumption that a shock from a high-pressure tank rupture is so

strong and thus propagates so fast that combustion, being a slower process, does not contribute to the blast wave strength. However, during the processing of available experimental data, the authors of this paper recently revealed that calculations by the established techniques (without taking combustion into account) do not reproduce the measured blast wave overpressures. This was especially pronounced in the case when the tank was located under the vehicle and a large amount of stored mechanical energy of compressed gas was spent to dislocate the vehicle from its initial position by about 22 m in this particular test.

This paper aims at understanding of the underlying physical phenomena, development and validation of an original model that allows the calculation of parameters of a blast wave from a tank rupture in a fire at different distances. Two typical cases of tank rupture in a fire are considered: a stand-alone hydrogen storage tank and a tank located under the vehicle. The effects on humans and civil structures at different distances from four typical hydrogen storage applications are estimated as examples of deterministic separation distance calculation using the model.

2.0 ENERGY STORED IN A HIGH-PRESSURE HYDROGEN TANK

2.1 Mechanical energy of a physical explosion

Let us use the definition of physical explosion given by Crowl who stated that "physical explosion occurs due to the sudden release of mechanical energy, such as by releasing a compressed gas, and does not involve a chemical reaction" [5]. There are several methods to calculate the energy of a physical explosion published elsewhere [5]: Brode's model [6], isentropic expansion model [7], isothermal expansion model [7], and thermodynamic availability model [8].

Brode's model [6]

The internal (mechanical) energy of ideal gas of mass, m, and temperature, T, which is compressed in a constant volume, can be written as $E_m=mc_vT$ [9]. Ideal gas equation of state is $pV=(m/M_g)RT$, and thus temperature is equal to $T=p/(\rho R/M_g)$. Based on the equality $R/M_g=c_p-c_v$, and the definition $\gamma=c_p/c_v$, the stored in a tank mechanical energy can be written then as:

$$E_m = c_v \frac{mp}{\rho(c_p - c_v)} = \frac{mp}{\rho(\gamma - 1)} = \frac{pV}{\gamma - 1}. \quad (1)$$

To account for an increase of gas pressure in the tank, p_g, compared to the surrounding pressure, p_s, in a volume V, the mechanical energy of compressed ideal gas can be expressed as (see for example Brode [6], Baker et al. [10]):

$$\Delta E_m = \frac{(p_g - p_s)V}{\gamma - 1}. \quad (2)$$

Isentropic expansion model [7]

Isentropic process is also called a reversible adiabatic expansion/compression process, i.e. there is no change in the entropy, $S=const$. The equation for reversible adiabatic expansion is $pV^{\gamma}=const$ [11]. The isentropic expansion model assumes an ideal gas expansion from its initial pressure in a tank, p_g, to the surrounding pressure, p_s [5]. Then, $p_s/p_g=(V_i/V_f)^{\gamma}$ (here $V_i=V$). Dividing ideal gas law equations for initial and final conditions gives: $(p_gV_i)/(p_sV_f)=T_i/T_f$. Thus, the relationship between temperatures and pressures is $T_f/T_i=(p_s/p_g)^{(\gamma-1)/\gamma}$.

According to the first law of thermodynamics the work performed by expanding gas of mass, m, in the adiabatic process is equal to the change of internal energy, i.e. $\Delta W=mc_v(T_i-T_f)$ [11]. As $R/M_g=(c_p-c_v)$ and $\gamma=c_p/c_v$, then $\gamma=1+(R/M_g)/c_v$ and thus, $c_v=(R/M_g)/(\gamma-1)$. Then, the work can be re-written as [11]:

$$\Delta W = m \cdot \frac{R/M_g}{\gamma - 1}\left(T_i - T_f\right) = \frac{1}{\gamma - 1}\left(p_g V - p_s V_f\right) = \frac{p_g V}{\gamma - 1}\left(1 - \frac{T_f}{T_i}\right) = \frac{p_g V}{\gamma - 1}\left[1 - \left(\frac{p_s}{p_g}\right)^{\frac{(\gamma-1)}{\gamma}}\right]. \quad (3)$$

This equation gives the work performed by compressed ideal gas in isentropic (reversible adiabatic) expansion from pressure p_g to p_s [7]. In the absence of heat losses in adiabatic process (ΔQ=0) the work performed by a system is equal to the change of internal energy, i.e. $\Delta W=\Delta E_m$.

Isothermal expansion model [7]

Isothermal process by definition requires *T=const*. Then, from the ideal gas law *pV=const* [11]. The work in isothermal process can be found as follows. By definition *dW=pdV*. As $V=(m/M_g)RT/p$, then $dV=-[(m/M_g)RT]dp/p^2$, and, therefore, the work differential is $dW=-[(m/M_g)RT]dp/p$. Then, the integration from the initial pressure in a tank, p_g, to the final pressure in the surroundings, p_s, gives $\Delta W=(m/M_g)RT\ln(p_g/p_s)$. Thus, the change of energy during isothermal expansion of compressed gas can be written as [5], [7]:

$$\Delta E_m = p_g V \cdot \ln\left(\frac{p_g}{p_s}\right). \quad (4)$$

It is worth noting that isothermal process is hardly applicable to a rapid expansion of gas from high to low pressure during a tank rupture. Indeed, this fast process of expansion is characterised by an essential temperature drop of the expanding gas as demonstrated experimentally. The higher the storage pressure, the larger is the temperature drop.

Thermodynamic availability model [8]

The thermodynamic availability (or batch availability) represents "the maximum mechanical energy extractable from a fixed mass of material as it reversibly moves into equilibrium with the environment" [6]. Authors think that this method is hardly applicable to explosion energy estimation as blast wave propagation time is much shorter than time needed for released gas to get into equilibrium with the surroundings. However, it is included here for comparison with other methods of physical explosion energy calculation [5].

The change in enthalpy of ideal gas as a function of temperature change (accounting for mass, *m*) is $\Delta H=mc_p\Delta T$ [8]. The entropy change for the ideal gas of mass, *m*, at a constant pressure is $\Delta S_{i\to f}=mc_p\ln(T_f/T_i)$ [8]. The entropy change at conditions when pressure changes is $\Delta S_{i\to f}=(m/M_g)R\ln(p_i/p_f)$ [8]. As the final pressure becomes equal with the pressure of surrounding, i.e. $p_f=p_s$, the change in the batch availability turns into [8]:

$$\Delta B = mc_p(T_f - T_i) - mc_p T_s \ln\left(\frac{T_f}{T_i}\right) - \frac{m}{M_g} RT_s \ln\left(\frac{p_i}{p_s}\right) - \frac{m}{M_g} RT_i\left[\left(\frac{p_s}{p_i}\right) - 1\right]. \quad (5)$$

Under the condition that the initial temperature in a tank is equal to the final one (surroundings), $T_i=T_f=T_s$, the batch availability reduces to $\Delta B=-(m/M_g)RT(\ln(p/p_s)-(1-p_s/p))$ [8]. Thus, in energy terms we have [5]:

$$\Delta E_m = p_g V\left[\ln\left(\frac{p_g}{p_s}\right) - \left(1 - \frac{p_s}{p_g}\right)\right]. \quad (6)$$

Comparison of compressed ideal gas mechanical energy calculated by different models

Figure 1 shows the mechanical energy of compressed hydrogen in a tank of 72.4 *L* volume as a function of storage pressure. The energy was calculated for the range of absolute pressure in the vessel from 0.1 to 100 MPa for ideal gas by use of different models described above.

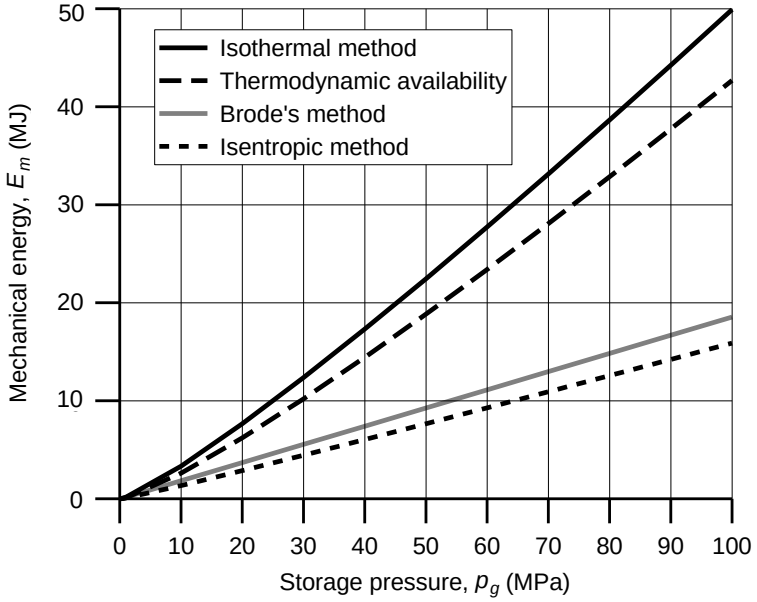

Figure 1. Mechanical energy of ideal compressed hydrogen gas in a tank of 72.4 *L* capacity as a function of storage pressure calculated by different models: Brode [6], isothermal and isentropic expansion [7], and thermodynamic availability [8].

Figure 1 demonstrates that there is an uttermost growth of the mechanical energy with pressure for the isothermal model. The calculation of energy by the thermodynamic availability model gives slightly lower energy. The isentropic model gives the lowest value of energy for the same pressure; however, it is quite close to the Brode's energy growth with pressure curve. The isothermal and thermodynamic availability models are built on the assumption that the temperature at the beginning and at the end of the process is the same. Thus, the "additional" energy is received from the surroundings after the cooled expanded gas gets the surrounding temperature. This results in more than twice larger energy per unit of a tank volume. However, the characteristic times of expansion of a compressed gas during the tank rupture and the heating up of the expanded gas by surroundings are different. Only the gas expansion has a characteristic time comparable with a blast wave propagation time, and thus can contribute to its strength. By this reason, both, isothermal and thermodynamic availability models are excluded from our further considerations. The isentropic model gives the lowest energy compared to other models. There is no any increase of energy due to heat transfer from the surroundings during adiabatic expansion, which is an idealisation of the real process. The Brode's model mechanical energy is close to the isentropic model, and this model is adopted here as the most realistic with less restricting assumptions.

2.2 Mechanical energy of compressed non-ideal (real) gas

Let us modify the Brode's approach to non-ideal gas using the Abel-Noble equation of state for real gas to improve a predictive capability of the model at high storage pressures, which are characteristic for hydrogen energy applications. It is widely recognised that the Abel-Noble equation works well for hydrogen. The equation is [12]:

$$p_g\left(1/\rho - b\right) = R/M_g \cdot T\,. \tag{7}$$

It can be re-written for temperature as $T=[p_g(1/\rho-b)]/[R/M_g]$. The total energy of compressed gas of mass, m, in a tank is $E_m=mc_vT$. Then, combining these two equations the energy for Abel-Noble gas can be written as $E_m=mc_vp_g(1/\rho-b)/(R/M_g)$. Using relationships $R/M_g=c_p-c_v$ and $\gamma=c_p/c_v$, the equation for mechanical energy of real gas can be written as:

$$E_m = mc_v \frac{p_g\left(1/\rho - b\right)}{c_p - c_v} = \frac{p_g\left(V - mb\right)}{\gamma - 1}. \tag{8}$$

Thus, the mechanical energy that will be released during tank rupture is:

$$\Delta E_m = \frac{\left(p_g - p_s\right)\cdot\left(V - mb\right)}{\gamma - 1}. \tag{9}$$

Hence, the mechanical energy of the compressed real gas is smaller than that of the ideal gas at the same storage pressures. Let us compare the performance of the previous model of mechanical energy for the ideal gas (Brode's model [6]) and the model derived here for the real gas. Figure 2 shows that with the growth of storage pressure the difference between energies for ideal gas and real gas increases. The over-prediction by the ideal gas model compared to real gas model is about 64% at 100 MPa. In spite of the conservatism of using the ideal gas law for calculation of mechanical energy, here we are interested in the improvement of the accuracy of mechanical energy model, which is a constituent part of the blast wave decay methodology described below. The mechanical energy of real gas will be used further in this study.

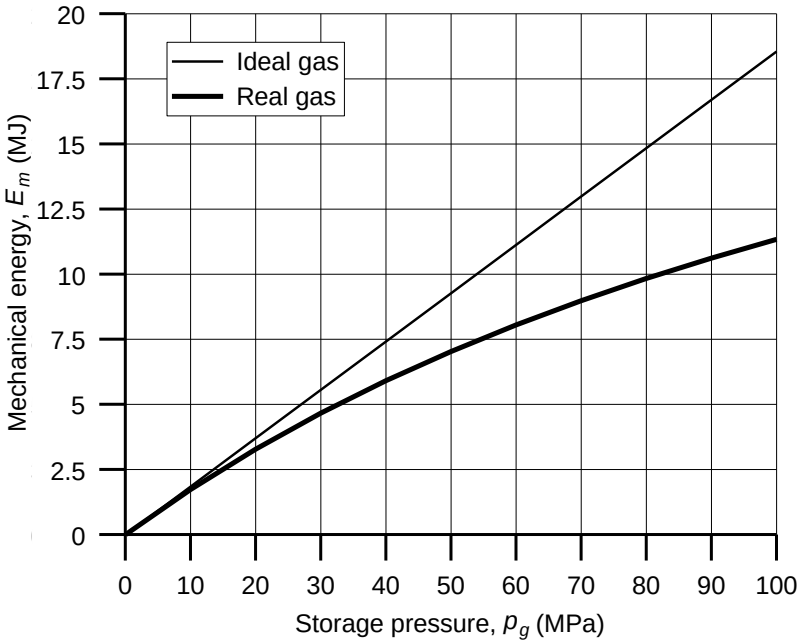

Figure 2. Mechanical energy as a function of storage pressures in a tank of 72.4 *L* capacity: thin line – ideal gas, bold line – real gas.

The mass of hydrogen can be calculated by the ideal gas equation of state as $m=pV/[(R/M_g)T]$. The mass of hydrogen stored in 72.4 *L* volume storage tank at pressure of 34.3 MPa (as in the stand-alone tank test used further in this work for validation of the methodology), calculated using the ideal gas equation, would be then m_g=2.01 kg. This is by 18% larger than the mass calculated using the Abel-Noble equation of state for real gas (m_g=1.654 kg).

2.3 Chemical energy (energy of combustion)

Up to now, the most widespread, if not the only, point of view has been: there is no contribution of combustion of released gas in air into the blast wave energy or it is negligible. Results of our work, presented here, disprove this concept, especially for an under-vehicle tank scenario.

The rupture of a tank with flammable gas in a fire will be accompanied by combustion of at least a part of released gas in air. Indeed, a shock wave propagating outwards from the tank through air generates a mixing of flammable gas (hydrogen) with air at the contact surface between gas and air due to high flow velocity behind the shock. The partially premixed combustion will take place, which comprises two modes: faster premixed combustion, and slower non-premixed (diffusion) combustion. A premixed part of the mixing layer at the contact surface, which is within the hydrogen flammability limits of 4-75% by volume, is expected to burn out faster than slower combustion of hydrogen in diffusion flamelets. Clearly, not all released hydrogen will burn out and contribute to the shock wave strength during its propagation, which is only the beginning of the longer combustion process ending by the fireball rising in the atmosphere by buoyancy. The non-premixed turbulent combustion of hydrogen at later stages of the fireball growth, when the shock wave is propagated far from the tank and already dissipated, would not practically contribute to the blast wave strength due to the "delayed" release of the chemical energy during the last stages of combustion.

Up to date, it is not clear whether or not the energy of combustion at the final stages of burning is contributing to the blast wave strength in the far field or not. However, this is possible in principle, as a glazing breakage in structures was observed sometimes at quite remote distances from the hydrogen-air deflagration site up to hundreds of meters. Experimental overpressures at large distances from a tank in the tests considered in this paper were not measured. Further analysis of this issue would be useful when new experiments are available.

3.0 EXPERIMENTS ON HYDROGEN STORAGE TANK RUPTURE IN A FIRE

3.1 Description of experiments

Two destructive bonfire tests with high-pressure hydrogen tanks, i.e. a stand-alone tank and an under-vehicle tank, in different experimental arrangements were performed and described by Weyandt in reports [13], [14] for the Motor Vehicle Fire Research Institute, and analysed in publications by Zalosh [4], [15] using available in literature correlations. Parameters of two storage tanks and test conditions are given in Table 1.

Table 1. Parameters of two storage tanks and test conditions.

Test	V, L	p_g, MPa	T_i, K	m, kg	a_g, m/s
Stand-alone tank [13]	72.4 [13]	34.3 [13]	300.15 [13]	1.654	1591
Under-vehicle tank [14]	88 [14]	31.8 [14]	306.15*	1.856	1581

Note: * accepted two degrees above the ambient temperature similar to test No.1 (stand-alone tank) [13] as temperature in the tank in test No.2 was not measured (ambient T_s=304.15 K [14]).

The mass of hydrogen in a tank, m_g, was calculated as $m_g=\rho V$, where density ρ was calculated by the Abel-Noble equation of real gas $\rho=p_g/(p_g b+R/M_g T_i)$. The speed of sound, a_g, was calculated using the equation of speed of sound for real gas presented in section 4.0.

In test No.1 (with the stand-alone tank) the heat release rate (HRR) of a propane fire was 370 kW (higher than in test No.2). The internal temperature and pressure in the tank increased only marginally during the fire before the rupture (due to low thermal conductivity of the tank shell material): from 27°C (300.15 K) to 39°C (312.15 K) and from 34.3 MPa to 35.7 MPa respectively. In test No.1 the tank ruptured in 6 min 27 s after the bonfire initiation. The largest tank projectile fragment was the 14

kg top half of the tank found 82 m away from the original tank location. Tank manufacturers and OEMs are developing engineering solutions to exclude such projectiles.

Blast wave overpressure was measured in the experiments by pressure transducers located at different distances and directions: parallel and perpendicular to the stand-alone tank axis (test No.1, see Figure 3, left), and in three directions for the under-vehicle tank test (test No.2, see Figure 3, centre).

The stand-alone tank test was carried out with Type 4 tank of 72.4 *L* capacity (84 cm long and 41 cm diameter) filled with hydrogen under initial pressure of 34.3 MPa and temperature 300.15 K. The mass of compressed hydrogen was estimated as 1.64 kg by Weyandt [13]. The mass calculated by authors using Abel-Noble equation of real gas is close to this estimate: 1.654 kg. The tank had a high-density polyethylene liner, carbon fibre reinforced polymer (CFRP) shell, and a fibreglass outer layer.

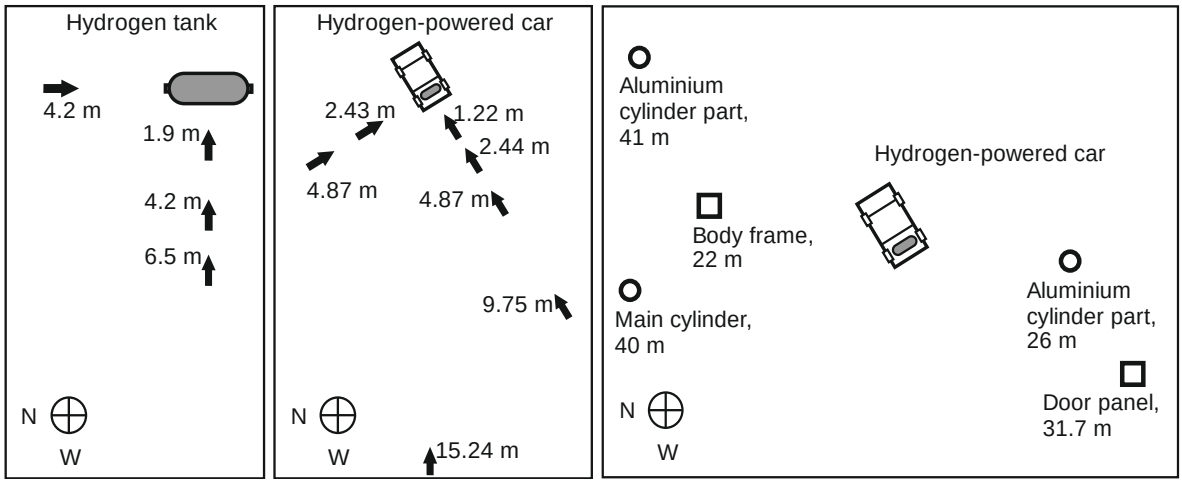

Figure 3. Location of pressure sensors in the stand-alone tank test No.1 (left), in the under-vehicle tank test No.2 (centre), and projectiles location for test No.2 (right). Adopted from Weyandt [13], [14].

The maximum measured overpressures at different distances from the stand-alone tank are as follows. West probes: 300 kPa (at 1.9 m), 83 kPa (4.2 m), and 41 kPa (6.5 m). A North probe: 62 kPa at 4.2 m [13]. The overpressure measured at distance of 4.2 m in West direction is about 35% higher than at the same distance of 4.2 m in North direction. This difference gives useful information about an order of experimental pressure "scatter" in different directions.

Test No.2 was carried out with a tank installed under a typical sport utility vehicle (SUV) of size $L_{SUV}\times W_{SUV}$=4.52×1.78 m at a distance of 28 cm above the ground. It was Type 3 tank (aluminium liner) of a somewhat larger capacity of 88 *L* compared to Type 4 tank in test No. 1, and the same outer dimensions of 84 cm long and 41 cm diameter as the tank in test No.1 (the difference in capacities can be attributed to a larger volume of polymeric liner compared to aluminium liner). Tank in test No.2 was filled with hydrogen under a slightly lower pressure of 31.8 MPa. The HRR of propane bonfire was in this case only 265 kW (by about 28% less than 370 kW in test No.1).

It is important to mention that in test No.2 the vehicle body frame was moved by 22 m being the "largest projectile". It was observed that "the rear of the vehicle projected upwards and twisted counter clockwise and over the front of the vehicle" and "the vehicle rotated clockwise about 90 degrees". A large tank fragment was found 41 m from the initial position of SUV. Fragment projectiles from the SUV were found at distances up to 107 m. It is possible that un-recovered fragments may have travelled even further. The locations of some projectiles are shown in Figure 3 (right). The maximum measured overpressures in the under-vehicle tank test are as follows: 140 kPa (rear of SUV at distance 1.22 m) and 80 kPa (side of SUV at distance 2.44 m).

More experimental observations are as follows. Burning of the tank composite layers started in 45 s (Type 4) and 20 s (Type 3) as observed by the black soot appearance. For the test with Type 3 tank

under the vehicle the earlier appearance of soot could be as well due to polymeric material in the SUV. Maximum fireball diameter of 7.6 m was observed for Type 4 tank at 45 ms after the tank rupture. Fireball lifted in 1 s. For Type 3 tank under the vehicle the fireball diameter was significantly larger - 24 m. A correlation applied by Zalosh [15] for the fireball diameter gave 9.4 m (for hydrogen mass of 1.64 kg). In both tests the duration of fireball was about 4.5 s (by IR video), and twice shorter by high-speed visible range cameras. A correlation applied by Zalosh [15] gave a shorter duration of only 0.6 s. This means that existing correlations, which were built on data for hydrocarbon fireballs, cannot be directly applied to hydrogen fireballs. More understanding of underpinning physical phenomena is needed to build new correlations for hydrogen safety engineering with higher predictive accuracy. Heat flux measured in test No.2 with Type 3 tank at distance 15.2 m in short spikes was in the range 210-300 kW/m^2 (for example, heat flux of about 35 kW/m^2 is characterised by 1% fatality in 10 seconds).

4.0 BLAST WAVE FROM A PRESSURISED TANK PHYSICAL EXPLOSION

This section describes a new methodology of a blast wave strength calculation in the case of physical explosion (no combustion) of a tank. The technique stems from the work by Baker et al. [10] but accounts for non-ideal gas effects. It allows the estimation of overpressure and impulse in a blast wave at different distances from the tank. The methodology can be used to calculate deterministic separation distances in the case of high-pressure gas tank physical explosion (rupture without combustion of released gas) by whatever reason.

There are several methods to calculate a blast wave for physical explosions, e.g. Shock Tube-TNT method, PROJEX method that also incorporates the Shock Tube-TNT method, the method by Baker et al., etc. that can be found elsewhere [16].

The overall process of estimation of the blast wave characteristics involves calculation of the initial shock and calculation of the blast wave in the near/far field. The initial shock (also called sometimes as the contact pressure) is assumed to take place when the vessel wall disappears instantaneously [16]. Thus, the contact pressure is of the highest value in the blast wave. Following the Baker's method one can estimate the initial shock, $\bar{P}_{st}$, by use of the Figure 4 below. A sought value of dimensionless starting shock overpressure is indicated on the right hand side of curves shown in Figure 4. The labels of $\bar{P}_{st}$ in Figure 4 that indicate a dimensionless starting shock value are shown at every other tick in the range from 40 to 100 (above 100 the values are not shown up to the last line of 140).

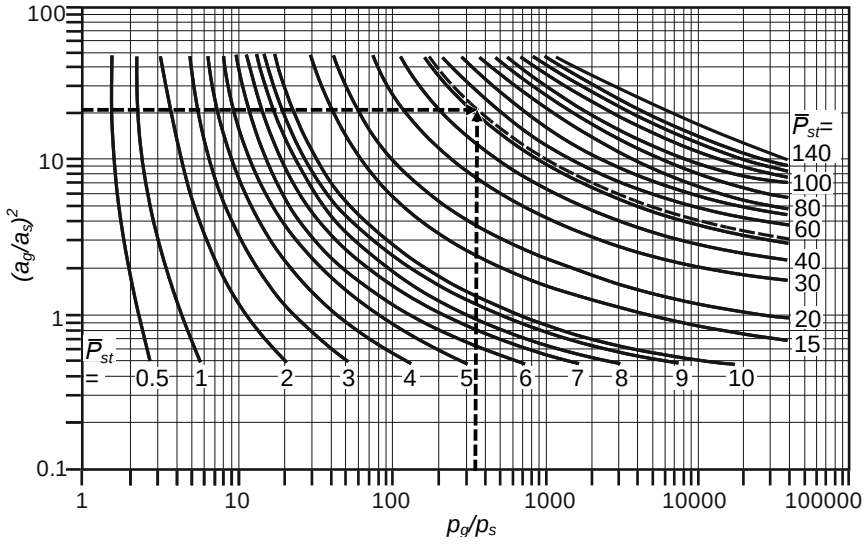

Figure 4. Graphical determination of the dimensionless starting shock overpressure, $\bar{P}_{st}$, by the squared ratio of the speeds of sound, $(a_g/a_s)^2$, and the ratio of the initial pressures, p_g/p_s (adopted from Baker et al. [10]).

To determine a dimensionless starting shock overpressure, $\bar{P}_{st}$, a squared ratio of the speeds of sound in compressed gas in the vessel and in the surrounding gas, $(a_g/a_s)^2$, and the ratio of initial pressures of the compressed gas and the surroundings, p_g/p_s, should be calculated. The speed of sound in the surrounding air can be calculated as for any other ideal gas [1]:

$$a_s = \sqrt{\gamma \frac{p_s}{\rho_s}}, \tag{10}$$

where γ is the ratio of specific heats for air, γ=1.4; p_s is the surrounding (atmospheric) pressure, which is assumed equal to p_s=1.013×10^5 Pa; ρ_a is the density of surrounding air. The density is calculated as $\rho_a=p_sM_a/RT$, where R/M_a=8.314 J/mol/K / 0.0289 kg/mol =287.7 J/kg/K (assuming the following air composition: 21% by volume of oxygen and 79% of nitrogen).

To account for non-ideal behaviour of compressed gas, e.g. hydrogen at pressures above 10-20 MPa, the speed of sound in Abel-Noble gas is calculated in this study as [1]:

$$a_g = \sqrt{\frac{\gamma \cdot p_g}{\rho_g \cdot (1 - b\rho_g)}}. \tag{11}$$

Let us analyse the stand-alone tank bonfire test [13]. Initial pressure in the vessel was p_g=34.3 MPa, and initial temperature of hydrogen in the tank was 27°C (300.15 K). Atmospheric air temperature was 25°C (298.15 K) that is two degrees below the temperature of hydrogen in the tank [13]. For hydrogen at high pressures, e.g. 35 MPa, the ratio of specific heats is γ=1.39 [17]. The density of air for test No.1 can be calculated as ρ_a=1.013×10^5 Pa/(287.7 J/kg/K·298.15 K)=1.18 kg/m^3. Thus, the speed of sound in surrounding air is 346.5 m/s at the test No.1 conditions. The speed of sound in hydrogen can be calculated as a_g=1591.33 m/s.

The squared ratio of the speeds of sound is then $(a_g/a_s)^2$=(1591.33/346.5)^2=21.09. The ratio of pressures is p_g/p_s=3.43×10^7/1.013×10^5=338.5. Thus, the sought non-dimensional starting shock overpressure is $\bar{P}_{st}$=52 (a dash line corresponding to the intersection of two arrowed lines in Figure 4). The dimensional starting shock overpressure is ΔP=52·1.013 kPa=5.27 MPa (calculated as $\Delta P=\bar{P}_{st}\cdot p_s$ [10]). It is worth noting that this is essentially below the storage pressure of p_g=34.3 MPa [13]. This is fully in line with the theory of pressure discontinuity decay when simultaneously with the shock propagating outward through air there is the rarefaction wave propagating inwards through the compressed gas in the tank.

There is another way to determine the dimensionless starting shock pressure, $\bar{P}_{st}$, i.e. to use one-dimensional gas dynamic equations that can be found elsewhere [18]. Firstly, the Mach number, M_{sh}, of the shock wave generated by the pressure discontinuity within and without the high-pressure storage tank is estimated using the equation:

$$\frac{p_i}{p_s} = \left(1 + \frac{2\gamma_s}{\gamma_s + 1}\left(M_{sh}^2 - 1\right)\right) \Big/ \left(1 - \frac{\gamma_g - 1}{\gamma_s + 1} \cdot \frac{a_s}{a_g} \cdot \frac{M_{sh}^2 - 1}{M_{sh}}\right)^{\frac{2\gamma_g}{\gamma_g - 1}}, \tag{12}$$

where p_i/p_s is the initial hydrogen to atmospheric air pressure ratio when the membrane is removed, γ_s and γ_g are specific heat ratios for air and pushing gas respectively (for our case γ_s = 1.4 and γ_g =1.39), a_s/a_g is the ratio of air to hydrogen speed of sound. Knowing M_{sh}, the dimensionless pressure behind the starting shock wave (propagating in air) can be calculated as:

$$\bar{P}_{st} = \left(\frac{2\gamma_s M_{sh}^2}{\gamma_s + 1} - \frac{\gamma_s - 1}{\gamma_s + 1} \right). \quad (13)$$

In further calculations we imply that temperature and pressure of hydrogen inside the vessel are those atmospheric before the fire. This assumption is based on the described above experimentally observed fact that changes in temperature and pressure within a tank at the moment of rupture are quite small. For example, in test No.1 hydrogen temperature and pressure both increased during the test by 4%. This allows the model to be applied for various hydrogen storage applications, when only the initial parameters are known. The difference in the model calculations with use of initial and final (just before the rupture) parameters of hydrogen in tests under consideration will be shown in section 7.4 as negligible. For scenarios with significant increase of temperature and pressure in a tank before rupture the value of these parameters before the rupture in a fire should be taken for calculations.

Figure 5 depicts the relationships of dimensionless overpressure and impulse versus dimensionless radius. The curves were generated by numerical simulations of spherical vessel bursts filled in with ideal gas [19]. Hydrogen at pressures of starting shock (typically below 10 MPa) can be considered as ideal gas. However, it is worth noting that the energy of compressed gas in the vessel is calculated in the updated methodology using real gas equation.

The determined value of $\bar{P}_{st}$ is used along with the dimensionless radius of the equivalent volume spherical vessel, $\bar{r}_v = r_v(p_s/E_m)^{1/3}$ [10], to identify a curve in Figure 5 (left), which correlates the dimensionless pressure in a blast wave, $\bar{P}$, and the dimensionless distance from a tank, $\bar{r}$ (to be defined later in this section). The mechanical energy, E_m, is calculated using the equation for real gas from section 2.2 as $E_m=[(p_g-p_s)(V-mb)]/(\gamma-1)=5.23$ MJ. For instance, for the stand-alone tank test, an equivalent volume spherical vessel radius, r_v, is calculated as $r_v=(3V/4\pi)^{1/3}=$ $(3\times0.0724/4\times3.14\ \text{m}^3)^{1/3}=0.26$ m, where V is the volume of the storage vessel. Then, the dimensionless vessel radius is calculated as $\bar{r}_v=0.26\ \text{m}\times(1.01\times10^5\ \text{Pa}\ /\ 5.23\times10^6\ \text{J})^{1/3}=5.7\times10^{-2}$.

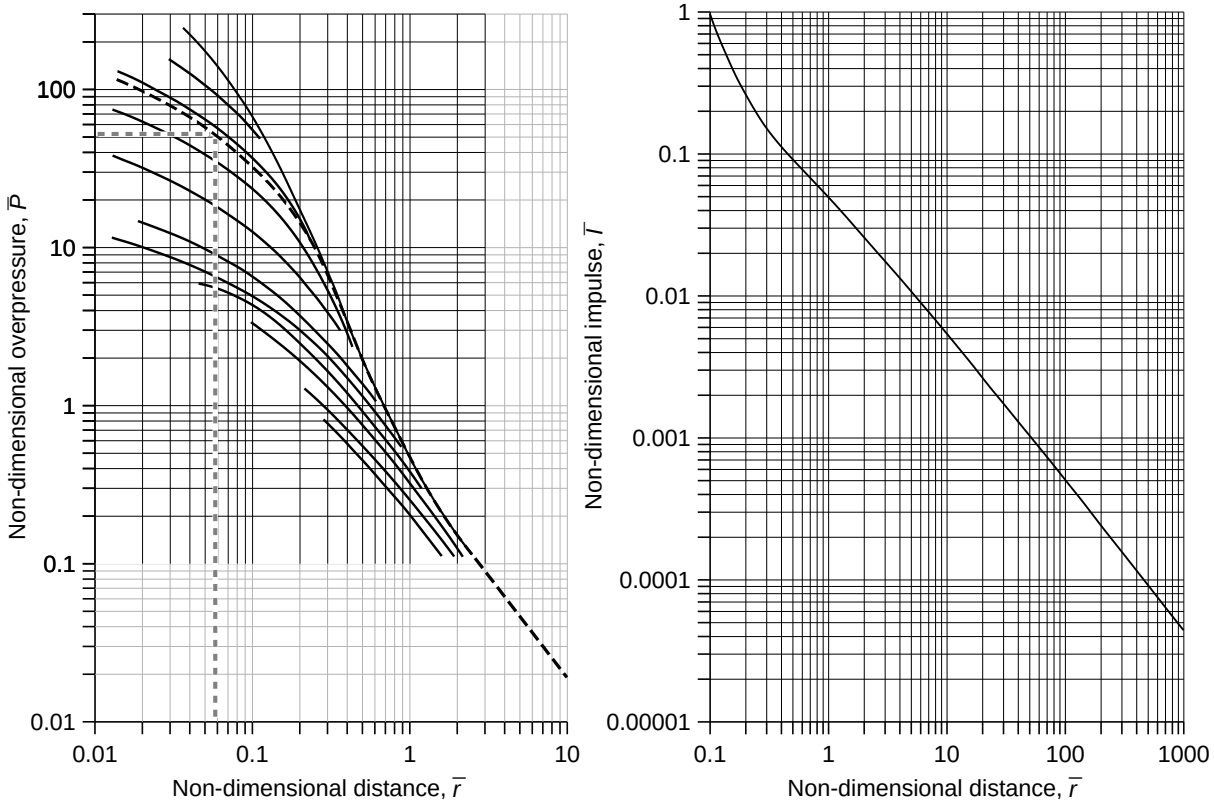

Figure 5. Left: dimensionless overpressure, $\bar{P}$, as a function of dimensionless distance, $\bar{r}$, with the identified for test No.1 black dash curve (at intersection of horizontal and vertical grey dash lines) and

extrapolated to lower non-dimensional overpressures by the black dash curve. Right: dimensionless impulse, $\bar{I}$, as a function of dimensionless distance, $\bar{r}$ [10].

The identified by dimensionless starting shock, $\bar{P}_{st}$, (horizontal grey dash line in Figure 5, left) and dimensionless vessel radius, $\bar{r}_v$, (vertical grey dash curve) black dash curve for test No.1 will then be used to find out the dimensional overpressure, P, at particular distances, r, from the tank or vice versa, i.e. determine a distance where the overpressure will have particular value. This identified new black dash curve is built as parallel to the nearest existing curve (see Figure 5, left). The dimensionless pressure-distance graph in Figure 5 (left) is extrapolated as well to lower overpressures compared to the original graph by Baker et al. [10] to enable predictions of lower dimensionless overpressures at farther distances from the vessel (this area is shown by grey grid lines in the graph, Figure 5, left).

Previously, the mechanical energy of compressed gas was calculated by Brode's equation [6] similar to Baker et al. [10], i.e. $\Delta E_m=(p_g-p_s)V/(\gamma-1)$. However, in this study we cannot use this equation without introduction of a systematic error due to non-ideal behaviour of hydrogen at high storage pressures up to 100 MPa in today's applications. The derived in this paper equation for the energy of compressed real gas, $\Delta E_{m=}(p_g-p_s)(V-mb)/(\gamma-1)$, is applied in all our further calculations.

The distance is usually dimensionalised as $\bar{r}=r(p_s/E_m)^{1/3}$ [10]. The technique is developed generally for the case of spherical symmetry, e.g. when an explosion takes place in the atmosphere far above the ground. However, in the case of explosion at the ground level, the whole amount of energy will be released into the hemisphere, due to reflection from the ground, rather than to the sphere. This means that a mechanical energy stored in a tank, E_m, should be doubled in calculations for the hemispherical geometry of explosion (physical explosion on the ground), i.e. it should be substituted by $2E_m$ to apply the methodology developed for the spherical symmetry. Baker et al. [10] described it as "if the ground acted like a perfectly smooth, rigid plane when explosions occurred on its surface, then it would reflect all energy at the ground plane". This is a conservative approach, which can be realised if the vessel rupture happened above the solid surface like concrete. Baker et al. [10] suggested also to use coefficient 1.8 instead of 2 as an explosion usually leads to cratering and a part of mechanical energy is consequently lost. We will apply the mechanical energy coefficient α=1.8 for comparison between model calculations and experimental data, because both tests were performed in the field and some losses of energy to displace the ground, i.e. for cratering, are expected. The same value of mechanical energy, i.e. the same geometry correction coefficient, should be applied to dimensionalise both $\bar{r}_v$ and $\bar{r}$.

To find out a dimensionless overpressure in a blast wave, $\bar{P}$, at a specified distance from the tank, r, the corresponding energy-scaled dimensionless distance, $\bar{r}$, should be calculated first:

$$\bar{r} = r\left(\frac{p_s}{\alpha \cdot E_m}\right)^{1/3}. \tag{14}$$

This equation shall be used to calculate the dimensionless radius and to find out the dimensionless impulse in Figure 5 (right). Further it is designated as $\bar{r}_I$. To convert the dimensionless overpressure, $\bar{P}$, into the dimensional overpressure in the blast wave, ΔP, it should be multiplied by the surrounding (atmospheric) pressure, p_s, as per definition $\Delta P=\bar{P}\cdot p_s$.

The impulse is the second essential parameter for the assessment of harmful pressure effects from a blast wave on humans and extent of structural damage or destruction [10]. Mathematically, the impulse is an integral of a blast wave pressure in time (area under the positive pressure-time curve, or area above the negative pressure-time curve). The impulse is dimensionalised as (the same mechanical energy correction factor, α, is applied here following the discussion above):

$$\bar{I} = \frac{I \cdot a_s}{(\alpha \cdot E_m)^{1/3} p_s^{2/3}}. \tag{15}$$

The non-dimensional impulse, $\bar{I}$, can be found graphically using Figure 5 (right) by a pre-calculated non-dimensional distance, $\bar{r}$. Then, non-dimensional impulse, $\bar{I}$, can be easily converted into dimensional impulse, I, using equation (15).

5.0 STAND-ALONE TANK FIRE TEST: MODEL WITHOUT COMBUSTION

Figure 6 (left) shows the effect of mechanical energy coefficients (α=1.8 and α=2.0) on the predictions of the blast wave for the real gas model and its comparison with experimental data for test No.1 (stand-alone tank). Over-prediction in the near-field (1.9 m) is by 6% and 18% for α=1.8 and α=2.0 respectively. Under-prediction at distance 6.5 m is by 31% for α=1.8, and by 28% for α=2.0. The predictions in the near field are closer to the experiment for α=1.8.

Figure 6 (right) presents the experimental data on a blast wave overpressure as a function of distance from the stand-alone hydrogen tank after its rupture in a fire [13] and overpressures calculated by two techniques (both without combustion) described in the previous section. One technique is for the real gas (this work) and another is for the ideal gas (Baker et al. [10]), both with α=1.8. The prediction of overpressures by the real gas technique in the near field (1.9 m) is very close to the experiment, while the ideal gas technique over-predicts by about 28%. For other distances the predictions by both techniques are close to each other and the experimental points.

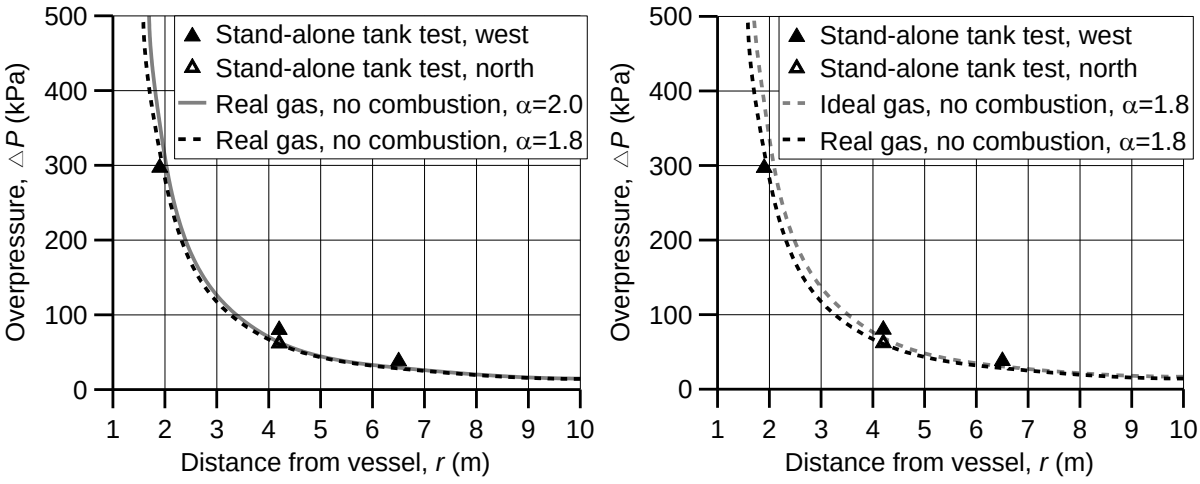

Figure 6. Comparison between experimental data in the stand-alone tank test [13] (triangles) and predictions by different methodologies without combustion. Left: predictions by the real gas methodology with different mechanical energy coefficients α. Right: predictions by the methodologies for the ideal gas and the real gas (both with α=1.8).

A following conclusion can be drawn from this comparison of experimental and calculated overpressures. The predictive capability of the technique without combustion can be improved by the inclusion of combustion contribution into the blast wave strength. Indeed, the combustion is expected to increase overpressure at farther distances from the tank, where the technique without combustion (physical explosion) gives some under-prediction.

6.0 UNDER-VEHICLE TANK FIRE TEST: MODEL WITHOUT COMBUSTION

The technique to calculate a blast wave overpressure without combustion contribution (physical explosion of a tank) is applied in this section to fire test No.2 with Type 3 tank, which was located under the Sport Utility Vehicle (SUV) [14]. Results are presented in Figure 7.

The straightforward application of the methodology without combustion with α=1.8 to the under-vehicle tank test demonstrates (see Figure 7) unrealistic over-prediction of the measured values of overpressure near the vehicle at distances less than 3 m, where first responders could operate, and under-prediction by about 30% in a far-field (at 15.24 m). The reason of considerable over-prediction

in the near field is obvious: a significant fraction of mechanical energy was spent onto the vehicle displacement (SUV body frame was found at distance of 22 m from its initial location [14]). Due to this loss of mechanical energy, it was found that a value of model parameter α, which would allow to match calculated overpressures with experimental at the closest to SUV measurement point (at 1.219 m), is comparatively small of α=0.14 (see lower dash curve in Figure 7). Expectedly, all other experimental overpressures are strongly under-predicted with this lower limit value of α=0.14. Table 2 shows the percentage of divergence of both calculations (with α=1.8 and α=0.14) from the experimental data.

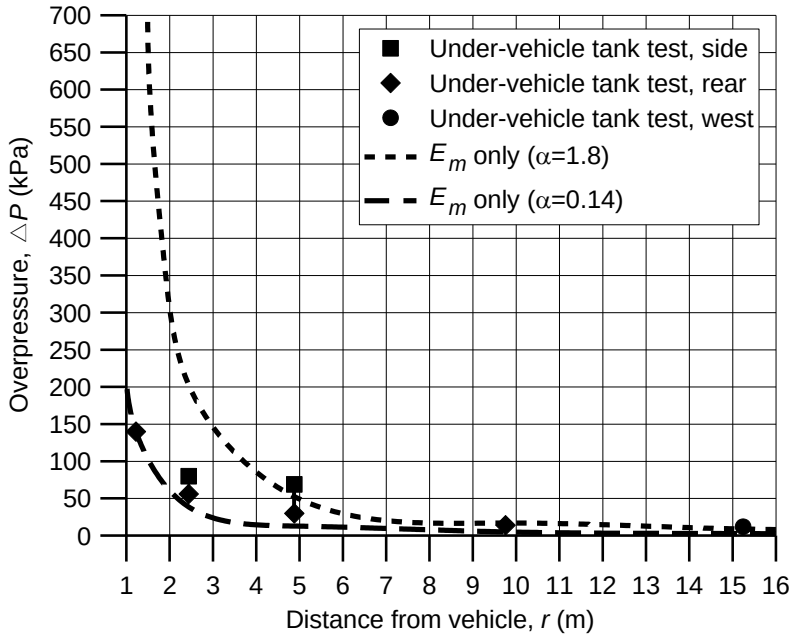

Figure 7. Experimental data on the blast wave decay for the under-vehicle tank test [14] (symbols), and overpressures calculated by the methodology without combustion with α=1.8 and α=0.14 (dash curves).

Table 2. Blast wave overpressures for the under-vehicle test: experiment versus calculations with two mechanical energy coefficients, α=1.8 and α=0.14.

Under-vehicle test No.2 [14]	Overpressure, ΔP (kPa), at different distances				
	r=1.22 m	r=2.44 m	r=4.88 m	r=9.75 m	r=15.24 m
Experiment	140	56-80	30-69	14	12
Calculation E_m only, α=1.8	1013.25 (+624%)*	202.65 (+261.8; +153%)**	52.69 (+75.6%; -23.6%)	16.72 (+19.4%)	8.85 (-26.3%)
Calculation E_m only, α=0.14	140.84 (+0.6%)	38.5 (-31.3%; -51.8%)	12.77 (-57.1; -81.3%)	4.86 (-65.3%)	2.68 (-77.7%)

Notes: * - percentage in parentheses corresponds to the deviation of a calculation from the experiment; ** - first and second percentage in parenthesis are deviations from the lower and the upper values of overpressure measured in the experiment respectively; +/- over-prediction and under-prediction of experimental overpressure respectively.

The analysis of Figure 7 demonstrates that the use of the methodology without combustion for the under-vehicle tank rupture in a fire is unacceptable. Indeed, it is found that the range of coefficient α is

extremely wide from 0.14 to 1.80 to partially match experimentally measured overpressures in only limited range of distances. In addition to this issue, there is a generic problem on how to choose value of α for arbitrary distance from a vehicle. It can be concluded that the existing technique for calculation of a blast wave decay with a constant value of mechanical energy coefficient, $\alpha=const$, without taking into account the contribution of combustion to the blast wave strength, has failed to reproduce the experimental data.

The conclusion out of Figure 7 analysis is that a value of α has to be small in the near-field and then has to increase with a distance from the centre of explosion to match the experimentally measured overpressures. This is a hint that there is an "unidentified" source of energy that feeds the blast wave as it propagates outwards. An obvious hypothesis that can be drawn from this observation is that this energy is chemical energy of turbulent non-premixed combustion of released hydrogen in the surrounding air. This combustion takes place at and behind the contact surface between air and hydrogen that follows the outward propagating shock wave. This hypothesis is applied in our study to build an original blast wave model accounting for combustion, which is able to reproduce experimental data and described in detail in the next section.

7.0 MODEL OF A BLAST WAVE DECAY: TANK RUPTURE IN A FIRE

7.1 Contribution of combustion into the blast wave strength

The performed in previous section analysis shows incapability of existing physical explosion techniques to predict accurately the experimentally measured overpressure in a blast wave from a hydrogen tank rupture in a fire. It is especially pronounced for the under-vehicle tank case. Our model is built on the assumption that the chemical energy, i.e. the energy of combustion of hydrogen released into air, has to be added dynamically to the mechanical energy of compressed hydrogen. Following the model, a new equation for non-dimensional distance is suggested for the calculation of overpressure in a blast wave, $\bar{r}_P$, that has to be applied when using Figure 5 (left):

$$\bar{r}_P = r\left(\frac{p_s}{\alpha \cdot E_m + \beta \cdot \left(\frac{r_{sh}}{r_b}\right)^3 \cdot E_{ch}}\right)^{1/3} . \qquad (16)$$

In this equation α is, as previously, the mechanical energy coefficient, and β is the chemical energy coefficient. The last indicates a fraction of combustion energy that is contributing into the blast wave strength during its travel to a particular distance, $r=r_{sh}$, where overpressure is probed. The empirical coefficient β accounts for the losses on radiation from the flame too.

The ratio $(r_{sh}/r_b)^3$ in the equations represents the ratio of the volume of hemisphere behind the shock, where the turbulent non-premixed combustion takes place and the chemical energy is being released, $2/3\pi r_{sh}^3$, to the volume of the hemisphere that could be occupied by products of complete combustion of hydrogen released from a vessel in air, $2/3\pi r_b^3$.

The model implies that for the blast wave strength calculation at different distances from the tank $r=r_{sh}$, i.e. at a distance where the shock is arrived, the following modelling conditions are applied. Equation (16) calculates the ratio $(r_{sh}/r_b)^3$ until the distance travelled by the shock, r_{sh}, is less or equal to the radius of the hemisphere which could be occupied by combustion products, r_b ($r_{sh} \le r_b$). The ratio of the radii, $(r_{sh}/r_b)^3$, increases monotonically up to its maximum value of $(r_{sh}/r_b)^3=1$ at $r_{sh}=r_b$ as a shock propagates outwards. The ratio $(r_{sh}/r_b)^3$ remains equal to 1 afterwards, when $r_{sh}>r_b$. More accurately, this ratio can be written as $[(r_{sh}-r_v)/r_b)]^3$ because the shock and thus the release of chemical energy are not possible for distances less than or equal to the vessel radius, r_v. However, due to small effect of this change on the overall predictive capability of the model it was abandoned.

There is an essential difference how the mechanical and chemical energies are treated in the model. While the empirical coefficient to mechanical energy is a constant α=const, the empirical coefficient to chemical energy is changing from 0 at the moment of tank rupture to its maximum value of β following the function: $\beta(r_{sh}/r_b)^3$. This is in compliance with the physics of the process as a tank rupture can be considered as an instant process compared to the slower process of following the shock propagation combustion.

The radius r_b is calculated in the model as follows. The volume of the hemisphere, occupied by combustion products formed after complete combustion of released hydrogen in air is $V_b=2/3\pi r_b^3$. The aforementioned volume is calculated as the volume of unburned stoichiometric mixture of air with released hydrogen, $V_u=2/3\pi r_u^3$, multiplied by an expansion coefficient of combustion products, i.e. E_i=6.85 for 30% hydrogen-air mixture [1]. Then, the radius of hemisphere occupied by the combustion products can be derived as $r_b=(3V_b/2\pi)^{1/3}$.

An example of calculations of a hemispherical volume occupied by an unburned stoichiometric hydrogen-air mixture, V_u, is given below. In the stand-alone tank test, the mass of stored hydrogen is m=1.654 kg. Thus, the number of moles contained in this amount of hydrogen is $n=m/M_g$=1.654 kg/2.016×10^{-3} kg/mol=820.26 mol. In the assumption of normal conditions 1 mole of any ideal gas occupies 22.4 L. Thus, 1.654 kg of hydrogen would occupy 820.26 mol×22.4 L/mol=1.84×10^4 L or 18.4 m^3. To find the amount of air needed for the complete combustion of this amount of hydrogen, let us write the reaction: $2H_2+(O_2+3.76N_2)=2H_2O+3.76N_2$. Thus, 1 mole of hydrogen consumes (1+3.76)/2=2.38 moles of air, i.e. in total 820.26×2.38=1952 moles of air will be needed for the combustion. Thus, the total amount is (1+2.38)=3.38 moles of hydrogen-air mixture per a mole of hydrogen. They would occupy 820.26 mol×3.38×22.4 L/mol=6.21×10^4 L or V_u=62.1 m^3. Thus, the radius of hemisphere with stoichiometric hydrogen-air mixture would be $r_u=(3V_u/2\pi)^{1/3}$=(3·62.1 m^3/2·3.14)$^{1/3}$=3.1 m. The radius of hemisphere occupied by the combustion products ($V_b=V_u\cdot E_i$=62.1 m^3·6.85=425.41 m^3) in test No.1 is then r_b=(3·425.41 m^3/2·3.14)$^{1/3}$=5.88 m (diameter 11.76 m).

The total mechanical energy of compressed hydrogen stored in the stand-alone tank in test No.1 is $E_m=[(p_g-p_s)\cdot(V-mb)]/(\gamma-1)$=[(3.43×10^7 Pa–1.013×10^5 Pa)·(7.24×10^{-2} m^3–1.654 kg·7.69×10^{-3} m^3/kg)]/(1.39–1)=5.23×10^6 J, i.e. E_m=5.23 MJ. Similar calculations for the under-vehicle tank give E_m=5.95 MJ. Thus, we can conclude that the total stored chemical energy, i.e. E_{ch}=198 MJ and E_{ch}=230.9 MJ respectively, is much higher than mechanical. The total chemical energy was calculated here as a hydrogen mass multiplied by hydrogen heat of combustion in air (lower heating value), e.g. in the stand-alone tank test it is $E_{ch}=m_g\times H_c$=1.654 kg·1.1993×10^8 J/kg=198 MJ.

The strength of a blast wave depends on an energy release rate rather than simply on the amount of energy (for example, the energy can be released so slow that practically no blast wave will be formed, e.g. in the case of comparatively slow release of the same amount of hydrogen through a pinhole in a tank). However, it is difficult to compare precisely release rates of mechanical and chemical energy in our case of a tank rupture accompanied by combustion. However, it is clear that while the mechanical energy releases practically "instantaneously", the chemical energy liberation during combustion behind the shock is a comparatively slower process. Only a part of the chemical energy can be feeding the shock during its propagation, the rest of combustion will be completed in the fireball after the strong shock wave is practically dissipated far away from the tank.

The model suggests that the combustion does not contribute significantly into the impulse of a blast wave, in contrast to the overpressure. The reasoning behind of this assumption is the growth of temperature behind the shock and thus generated by combustion acoustic waves will feed the leading shock rather than to increase the overpressure along the whole pressure transient. The comparison of the impulse calculated by the model with experimental impulse is presented further in this paper. The equation of the dimensionless distance, $\bar{r}_I=r[p_s/\alpha\cdot E_m]^{1/3}$, is applied for the calculation of dimensionless impulse in Figure 5 (right).

7.2 Stand-alone tank fire test: the model with combustion

Figure 8 compares the experimentally measured overpressures during the blast way decay with calculations by two models. One is the real gas model without combustion (mechanical energy only, dash grey curve), and another is the real gas model with combustion using the combined energy scaled radius as described in the previous section (solid black curve).

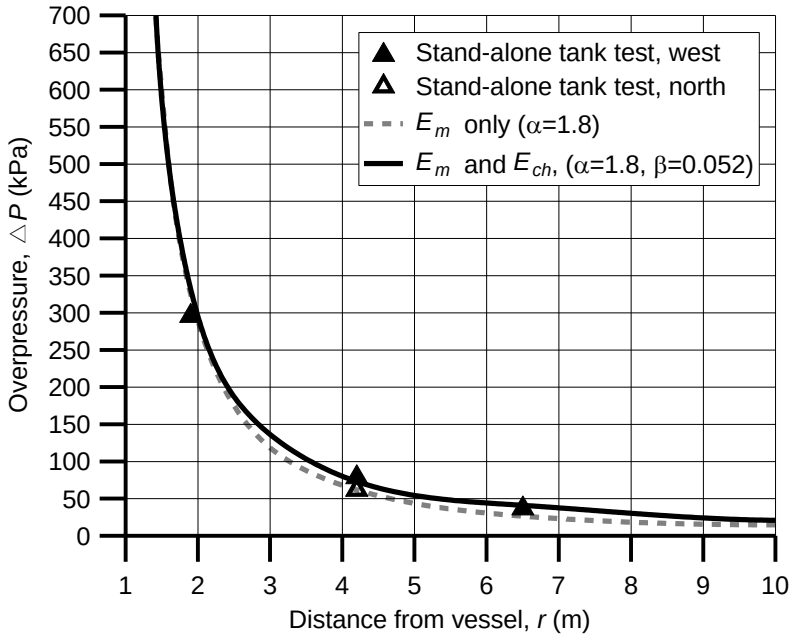

Figure 8. Experimental data on the blast wave decay in the stand-alone tank fire test [13] (triangles), and calculations by the real gas model without combustion (α=1.8, dash grey curve), and the real gas model with combustion (α=1.8 and β=0.052, solid black curve).

Table 3 shows the experimental and calculated overpressures for models without and with contribution of combustion into the blast wave strength for the stand-alone tank fire test No.1.

Table 3. Experimental data versus calculations with scaling by mechanical energy only (α=1.8), and scaling by both mechanical and chemical energy (α=1.8, β=0.052) for test No.1.

Stand-alone tank fire test No.1	Overpressure, ΔP (kPa), at different distances, r (m)		
	r=1.9 m	r=4.2 m	r=6.5 m
Experiment [13]	300	62-83	41
Scaling: E_m only (α=1.8)	319.2 (+8.4%)	60.8 (-0.3%; -27%)	28.37 (-31%)
Scaling: E_m (α=1.8) and E_{ch} (β=0.052)	332.3 (+10.8%)	72.9 (+17.6%; -12.2%)	41 (0%)

Table 3 demonstrates that the model with mechanical energy only has over-predicted the overpressure at 1.9 m by 8.4%, and under-predicted it at 4.2 m and 6.5 m by 0.3% and 35.7% respectively. Calculations by the model with mechanical and chemical energies give a marginally higher over-prediction of overpressure at 1.9 m by 10.8%. However, the calculated overpressure passes the test data range of 62-83 kPa at 4.2 m with value 72.9 kPa (between two experimental points), and exactly matches the measured overpressure at 6.5 m.

Determined by the inverse problem method the empirical coefficient for chemical energy in the stand-alone tank test is β=0.052. Thus, only a small fraction of the total chemical energy of about 5.2% has contributed into the blast wave strength during its propagation. The addition of this "small" fraction of

the combustion energy into the model has allowed an adequate prediction of the measured blast wave overpressures throughout the near-field and the far-field distances from the tank. It can be concluded, that the developed model with combustion ensures a better predictive capability of the blast wave decay compared to the model without combustion.

7.3 Under-vehicle tank fire test: the model with combustion

Figure 9 compares experimental overpressures from the under-vehicle tank rupture in the fire test (symbols) against predictions by two models: the real gas model without combustion (two dash grey curves), and the real gas model with combustion (solid black curve). It can be seen that the inclusion of combustion energy into the energy scaled radius has improved the predictive capability of the blast wave model drastically.

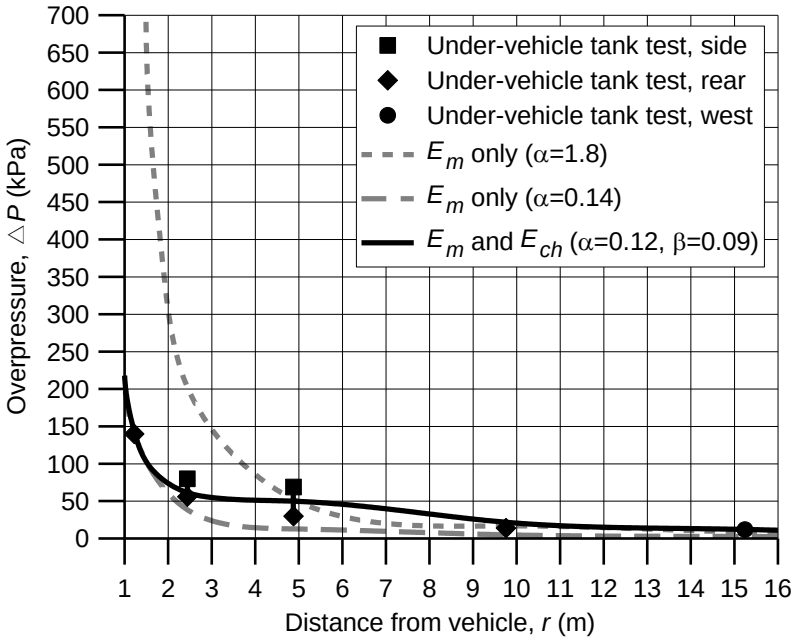

Figure 9. Experimental data on the blast wave decay in the under-vehicle tank test No.2 [14] (symbols); predictions by the real gas model without combustion (two dash grey curves); and prediction by the real gas model with combustion (solid black line).

It is worth noting that the model with combustion has reproduced even the experimentally observed "plateau" of the blast wave overpressure at distances 2.5-5.5 m from the tank. The existence of the "plateau" in the experiment is a fact. The existence of the "plateau" in the theory can be explained as follows. The radius of hemisphere occupied by the combustion products can be calculated for test No.2 as r_b =6.1 m. This means that the contribution of combustion into the blast wave is growing proportional to the radius cubed until it propagates to 6.1 m from the explosion source, when the chemical energy coefficient reaches its maximum value of β=0.09.

What are fractions of stored mechanical and chemical energy contributing to the blast wave strength? The fraction of mechanical energy transferred to the blast wave in the under-vehicle tank test is α=0.12 (this is 15 times smaller than in the stand-alone tank test with α=1.80!) and the fraction of chemical energy is of the same order, i.e. β=0.09 (about twice larger than for the stand-alone tank test). Thus, in the under-vehicle tank test the total amount of mechanical energy contributing to the blast wave can be estimated as $\alpha \cdot E_m$=0.12·5.95 MJ=0.7 MJ. The total amount of chemical energy feeding the blast wave due to combustion is $\beta \cdot E_{ch}$=0.09·230.9 MJ=20.8 MJ, i.e. about 30 times larger than the fraction of mechanical energy contributing to the blast wave.

It is worth mentioning that in the near-field a ratio of chemical to mechanical energy contributing to the blast wave increases gradually from 0 at distance of the tank radius to 30 at and after r_b=6.1 m (as

the chemical energy is released not instantly). It can be concluded that in the under-vehicle tank test at distances longer than r_b=6.1 m, it is exactly the combustion process that defines the blast wave strength. Contrary, in the stand-alone tank test the fractions of chemical to mechanical energy feeding the blast wave are close to each other: αE_m = 1.8·5.23 MJ = 7.33 MJ, and βE_{ch} = 0.052·198 MJ = 10.3 MJ. Thus, the previous "knowledge" that there is no contribution of combustion to the blast wave strength generated by high-pressure tank rupture in a fire is obsolete.

For the model without combustion there are two dash curves with two different mechanical energy coefficients in Figure 9. The decrease of the mechanical energy coefficient from α=1.8 (as in the stand-alone tank test) to α=0.14 (the curve is built to reproduce the overpressure in the near-field at location of 1.219 m) is due to losses of the mechanical energy to damage and displace the vehicle by 22 m from its initial position and scattering of numerous projectiles (up to 107 m [14]). Determined by the inverse problem method in the model with combustion the mechanical energy coefficient is α=0.12. This is close to the model without combustion for the under-vehicle tank test in the near-field, i.e. α=0.14.

The increase of the chemical energy fraction coefficient from β=0.052 (the stand-alone tank test) to β=0.09 (the under-vehicle tank test) is thought to be due to an enhanced mixing and thus combustion of hydrogen in air by the vehicle frame and its parts playing a role of turbulising obstacles. In addition to this, the blast wave in test No.2 due to losses is weaker in the near-filed compared to test No.1, and hence propagates slower. By this reason, there is more time for combustion to contribute to the blast wave strength. Table 4 compares the experimental data on the blast wave overpressures for the under-vehicle tank test with values calculated by models with different scaling (see also Figure 9).

Table 4. Blast wave overpressures in the under-vehicle tank test No.2: experiment versus calculations by the model with mechanical energy only (α=1.8, and α=0.14), and combined mechanical and chemical energy scaling (α=0.12, β=0.09).

Under-vehicle tank test No.2	Overpressure, ΔP (kPa), at different distances, r (m)				
	r=1.22 m	r=2.44 m	r=4.88 m	r=9.75 m	r=15.24 m
Experiment [14]	140	56-80	30-69	14	12
Scaling: E_m only (α=1.8)	1013.25 (+624%)*	202.65 (+261.8; +153%)**	52.69 (+75.6%; -23.6%)	16.72 (+19.4%)	8.85 (-26.3%)
Scaling: E_m only (α=0.14)	140.84 (+0.6%)	38.5 (-31.3%; -51.8%)	12.77 (-57.1; -81.3%)	4.86 (-65.3%)	2.68 (-77.7%)
Scaling: E_m (α=0.12) and E_{ch} (β=0.09)	143.9 (+2.8%)	61.2 (+9.3%; -23.5%)	49.65 (+65.5%; -28%)	21.8 (+55.7%)	11.96 (-0.3%)

7.4 Effect of initial hydrogen temperature and pressure on a blast wave strength

During the stand-alone tank fire test the temperature and pressure of hydrogen somewhat changed from those at the start of experiment. To the moment of tank rupture (the end of test parameters) temperature changes from 300 K to 312 K, and pressure raised from 34.3 MPa to 35.7 MPa [13], i.e. both increased by about 4% to initial values. Figure 10 and Table 5 demonstrate that accounting for the change in initial temperature and pressure of hydrogen before the tank burst, makes a little difference and can be neglected for a simplification of the blast wave calculation methodology.

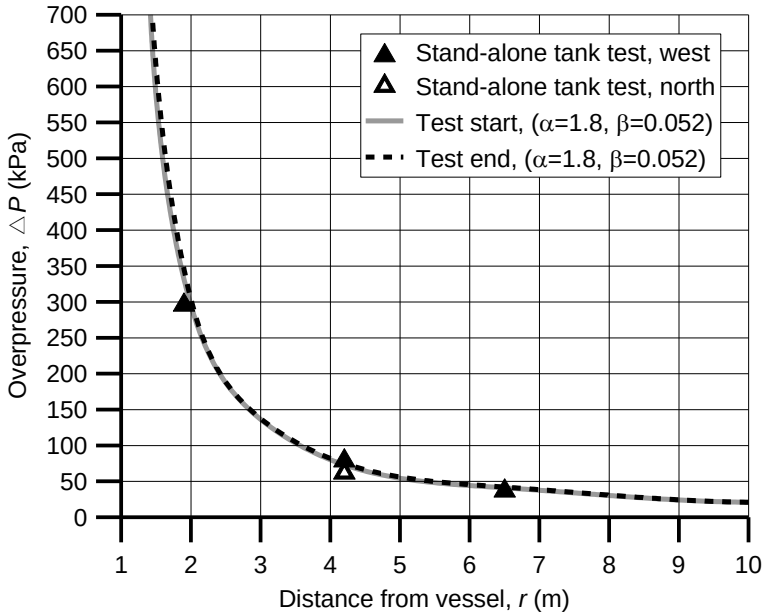

Figure 10. Blast wave decay in the stand-alone tank test No.1: prediction by the model with hydrogen temperature and pressure at the start of the test, 300 K and 34.3 MPa respectively (grey solid curve); and prediction by the model with parameters at the moment of tank rupture, 312 K and 35.7 MPa (black dash curve).

Table 5. The stand-alone tank test: experimental data versus calculations with scaling by mechanical energy only (α=1.8), and mechanical and chemical energy (α=1.8, β=0.052).

Stand-alone tank test No.1	Overpressure, ΔP, (kPa), at different distances		
	r=1.9 m	r=4.2 m	r=6.5 m
Experiment [13]	300	62-83	41
Test start parameters	332.3 (+11%)	72.9 (+18%; -12%)	41 (0%)
Test end parameters	346.5 (+15%)	74.9 (+21%; -10%)	42.05 (+2.5%)

The comparison of the effect of hydrogen parameters at the start and at the end of the test is possible for the stand-alone tank test only. The internal tank pressure was not measured in the under-vehicle test. It was explained as: "The internal pressure of the hydrogen cylinder remained fairly constant during the exposure. The pressure transducer failed at approximately 1 min 24 sec into the test, at which time the cylinder pressure had not changed from its initial value" [14].

7.5 Use of experimentally observed fireball size in the model

The maximum diameter of visible fireball in the stand-alone tank test was reported as 7.6 m [13]. The developed model is based on the calculation of a hemisphere diameter occupied by combustion products of stoichiometric hydrogen-air mixture. The calculated diameter of this hemisphere is the maximum distance until which the release of chemical energy contributing to the blast wave strength is accounted for in the model. For the stand-alone tank test it is calculated as 11.76 m. This is by 55% larger compared to the experimentally observed fireball diameter. This can probably be explained by an incomplete combustion of hydrogen in air, or by cooling of outer boundary layer of combustion products during turbulent mixing with cold surrounding air, or by known poor luminosity of hydrogen flame, or by all these factors together.

The maximum fireball diameter observed in the under-vehicle tank test was significantly larger - 24 m [14]. The model gives the size of the combustion products hemisphere of about twice smaller diameter of 12.22 m. This difference could be explained by the following possible reasons. First of all, reacting

in air hydrogen jets from beneath the vehicle could erode and entrain soil particles that will burn and irradiate at longer distances compared to hydrogen flame itself. “Flying” vehicle creates different conditions for hydrogen dispersion, mixing and combustion. The congestion can facilitated an appearance of jet flames with a larger initial momentum compared to the conditions of uncongested tank test No.1.

Let us estimate the difference in the blast wave overpressure prediction by using the fireball radius data observed in the test and calculated by radius of the hemisphere occupied by combustion products, r_b, following the developed model. Figure 11 shows the results for tests No.1 and No.2, left and right graph respectively. For the stand-alone tank test No.1 (Figure 11, left) the somewhat different in the near-field up to about 5 m indicating that the overpressure would increase if the smaller fireball diameter from the experiment is applied. Figure 11 (left) shows that the use of observed in the test fireball diameter for the stand-alone tank test over-predicts experimental data at 1.9 m (west) by about 20%; at distance 4.2 m the calculated value is 96.3 kPa, which is larger than the experimental overpressure 62 kPa by 35.6%, and at distance 4.2 m an over-prediction of experimental data of 83 kPa is by 13.8%; the experimental fireball approach gave an over-prediction 1.3% at distance 6.5 m. It is worth mentioning that the accuracy of experimental fireball size measurement is poor due to different reasons, including those mentioned above in this section. The use of the model assumption that the maximum radius, where combustion contributes to the blast wave, is equal to the radius of combustion products of stoichiometric combustion of hydrogen in air eliminates this experimental uncertainty, and predicts the experimental data with higher accuracy.

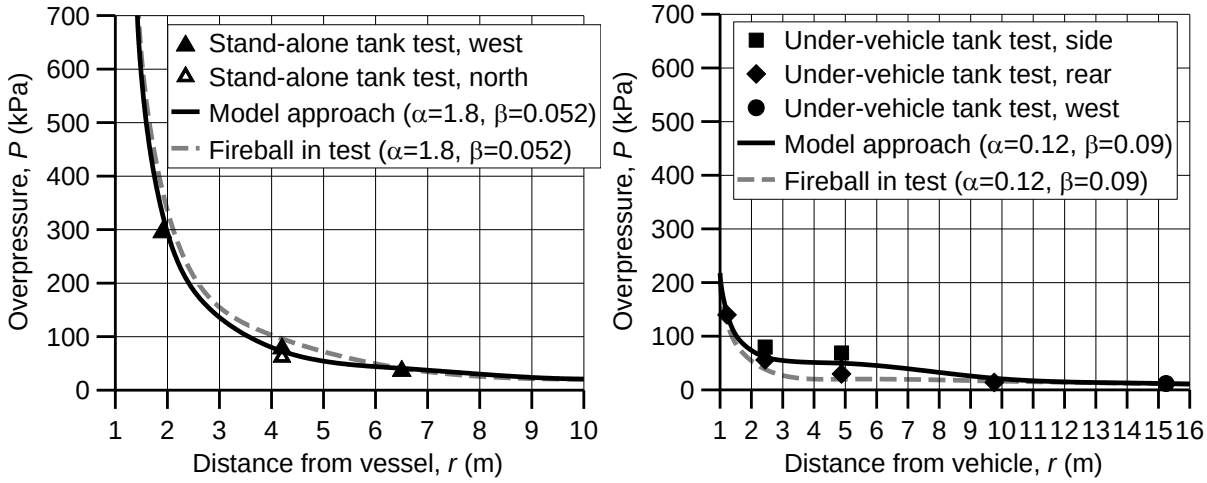

Figure 11. Blast wave decay in the stand-alone tank fire test (left) and the under-vehicle tank test (right): the model approach (solid black line), and the approach with the use of experimentally observed fireball radius (dash grey line).

Figure 11 (right) demonstrates that the model with the use of experimentally observed fireball radius instead of r_b gives a noticeable under-prediction of experimental overpressures in the under-vehicle tank fire test as follows: at 1.219 m by 9.6%; at 2.438 m the under-prediction is by 32% (relative to the lower rear of the vehicle test data point); at 4.877 m it is by 34% (to the lower rear test data point); at 9.754 m the over-prediction is by 15%; at 15.24 m under-prediction is by 8%.

Thus, the alteration of the developed technique by using experimentally observed fireball radius and recalibration of values of α and β seems meaningless. Indeed, there are currently no methods able to predict experimentally observed fireball radius accurately. Probably this is impossible at all as fireball size can be affected by a large number of unknown parameters and phenomena mentioned above, e.g. combustion of entrained materials, etc.

The conclusion of this section is that the developed model, based on the radius of hemisphere filled with combustion products of complete combustion of the released hydrogen in air, r_b, is the robust

model to be applied in blast wave decay calculations as a part of hydrogen safety engineering process. The model reproduces the experimentally observed overpressures more accurately compared to the case of taking r_b as an experimentally observed fireball size.

7.6 Comparison of experimental and calculated impulse in blast waves

Besides the overpressure, the impulse plays a vital role in the assessment of effects produced by a blast wave on humans and structures. The dimensionless impulse, $\bar{I}=I\cdot a_s/[(\alpha\cdot E_m)^{1/3}\cdot p_s^{2/3}]$, and dimensionless radius, $\bar{r}_I=r[p_s/(\alpha\cdot E_m)]^{1/3}$, are used to work with the graph in Figure 5 (right). Dimensional impulse is calculated by equation $I=\bar{I}\,[p_s^{2/3}\,(\alpha\cdot E_m)^{1/3}]/a_s$.

Figure 12 shows the experimental (symbols) and calculated (lines) impulse in the blast waves for two tests under consideration. The experimental values of impulse were calculated by processing the experimental pressure transients available from Weyandt's reports [13], [14].

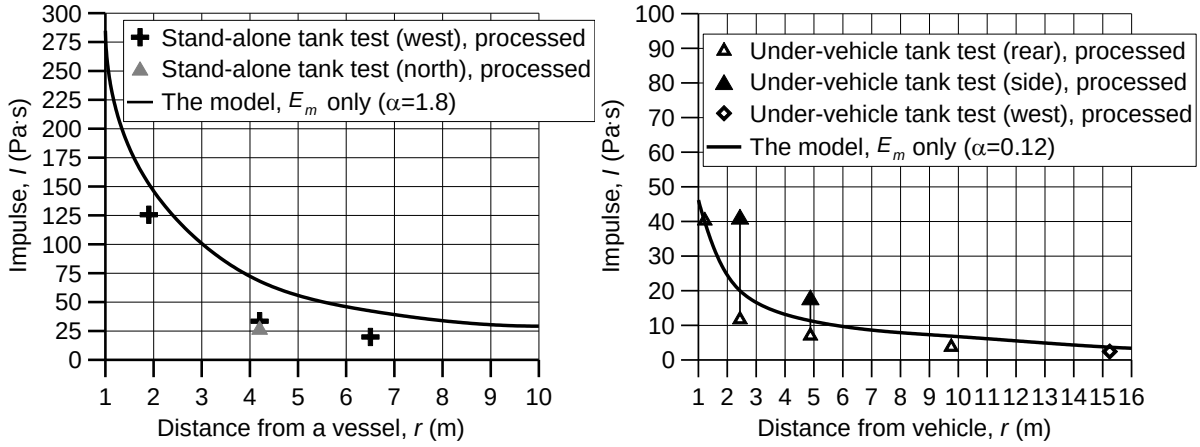

Figure 12. Blast wave impulse measured in the test (symbols) and calculated by the methodology (curves): the stand-alone tank test (left); the under-vehicle tank test (right).

Figure 12 (left) shows that the model gives a conservative prediction of the impulse in the stand-alone tank test: at the near-field (1.9 m) it over-predicts the experiment by 21%; at 4.2 m the over-prediction is 144% and 104% respectively; at 6.5 m it is 113%. Figure 12 (right) demonstrates that in the under-vehicle tank test the model slightly over-predicts the near-field point (1.219 m) by 0.7%; at 2.438 m, the calculated impulse is between the lower and upper values of experimental impulse (the differences is +70% and -52% respectively); at 4.87 m these differences are +63% and -37%; at 9.75 m and 15.24 m the model gives over-prediction by 85% and 57% respectively. Thus, we can conclude that the methodology is able to reproduce the experimentally measured impulses in the blast waves of two tests with a reasonable accuracy.

8.0 HARMFUL PRESSURE EFFECTS ON HUMANS AND DAMAGE CRITERIA FOR STRUCTURES

This section overviews the data on harm criteria on humans and damage to civil structures from a blast wave. The combined effect of overpressure and impulse on humans and buildings is presented graphically. Examples of the deterministic separation distance calculation using the model are shown for a number of typical hydrogen applications. It should be especially underlined that the selected in this study harm criteria for humans and damage criteria for buildings are subjective choice of the authors and do not represent a part of any regulations, codes or standards. They are rather results of the authors' analysis of published data and could be considered as a general guideline only.

8.1 Harmful pressure effects on humans

Harm to humans from a blast wave include eardrum rupture, lungs damage, translation of a body with all possible negative consequences like hitting a wall or a floor, etc. Harmful effects depend on the combination of overpressure and impulse as compiled in Figure 13 (left) following Baker et al. [10], [19]. For gaseous explosions like deflagration in the open atmosphere, the impulse, which is the integral of overpressure over time, can be positive or negative, depending on a phase of the pressure transient. For hydrogen-air deflagrations the peak of negative phase is often larger than the positive phase peak. There is little negative phase in pressure transients from high explosives.

Harm effects from a blast wave generated by high explosive, documented by Baker et al. [10], [19], could be different from harm effects of blast wave produced by a high pressure tank rupture in a fire. Due to the absence of data on harmful effects on humans and damage to structures specific for high-pressure tank rupture we adopt published data for high explosives [10], [19].

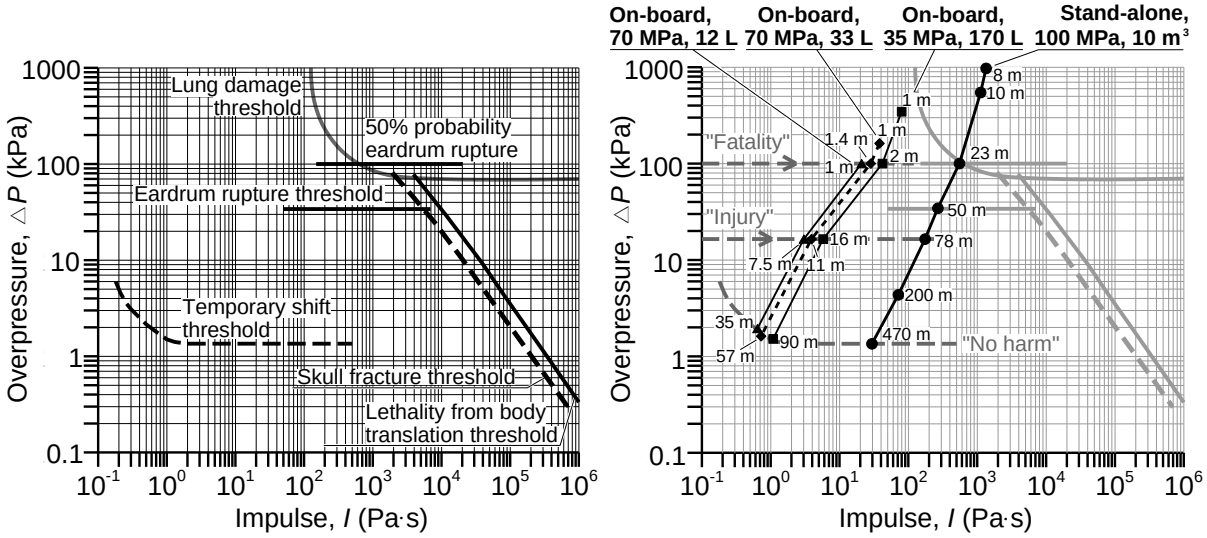

Figure 13. Left: overpressure-impulse thresholds of harm criteria for humans, adopted from Baker et al. [10], [19]. Right: pathways of blast wave decay from tank rupture in a fire for a number of typical hydrogen storage applications.

The temporary threshold shift curve in Figure 13 (left) describes a temporary loss of hearing [10] that occurs at overpressure above 1.35 kPa and impulses above 1 Pa·s. This will be considered as a threshold for no harm to humans, i.e. it will be applied here to calculate the "***no harm"*** deterministic separation distance (see grey "No harm" dash line in Figure 13, right).

Following Baker et al. [19] the threshold for eardrum rupture requires an overpressure of 34 kPa and the impulse above 50 Pa·s. The probability of 50% of eardrum rupture is associated with the overpressure of 100 kPa and the impulse up to 0.15 kPa·s. These data were generated mainly based on the high explosives events. Thresholds for physical explosions of high-pressure tanks followed by combustion might be different. This probably explains why different overpressures for eardrum rupture could be found in the literature. For example, 1% eardrum rupture threshold of 16.5 kPa is stated in [20]. This is below the Baker's "eardrum rupture threshold" of 34 kPa, and does not assign any particular impulse range (eardrum rupture threshold [10] has the impulse range along with the overpressure threshold). Using a conservative approach we define here 16.5 kPa as the injury threshold for humans from a direct effect of pressure wave (humans could be injured by pieces of window glasses at lower overpressures, etc.). Thus, an overpressure of 16.5 kPa will be applied in this study to define the ***"injury"*** deterministic separation distance (indicated by grey arrowed line in Figure 13, right). More information of harmful pressure effect on humans outdoors is provided in Table 6 [20].

Table 6. Harmful pressure effects on humans outdoors [20].

Harmful effect	Overpressure, kPa	Impulse, kPa·s
Threshold for skin laceration from flying glass	6.9-13.8	0.512
Threshold for serious wound from flying glass	13.8-20.7	1.024
1% eardrum rupture probability *	16.5	-
50% serious wound from flying glass	27.6-34.5	1.877
50% probability of eardrum rupture	43.5	-
Near 100% serious wound from flying glass	48.3-55.16	3.071
90% probability of eardrum rupture	84	-
1% probability of fatality due to lung haemorrhage **	100	-
50% probability of fatality due to lung haemorrhage	140	-
99% probability of fatality due to lung haemorrhage	200	-

Notes: * - threshold for calculation of the ***"injury"*** deterministic separation distance; ** - threshold for calculation of the ***"fatality"*** deterministic separation distance.

Lung damage, skull fracture and lethality effects are plotted in Figure 13 (left) considering the human body weight of 60 kg. The threshold for lung damage requires an impulse of about 0.125 kPa·s and quite high overpressure; with the increase of impulse above 0.125 kPa·s the curve decreases down by pressure to the value of about 70 kPa at impulse above 1 kPa·s. This is close to the overpressure value of 100 kPa for "1% probability of fatality due to lung haemorrhage" [20] (shown by arrowed grey dash line in Figure 13, right). This overpressure is applied further in this study for calculation of the ***"fatality"*** deterministic separation distance for four typical hydrogen storage tank applications described below. The choice of overpressure threshold for the "fatality" is similar for the "injury" threshold, i.e. both are selected as 1% probability of either eardrum rupture or fatality due to lung haemorrhage. The thresholds for skull fracture and lethality from body translation are shown by two parallel lines in Figure 13 (left). The key factor here is the impulse of about 1.9 kPa·s and 3.9 kPa·s respectively. With the increase of impulse, the overpressure thresholds decrease from 81 kPa to 0.3 kPa and from 78 kPa to 0.2 kPa respectively.

There are various harm criteria for humans that can be found elsewhere, e.g. [21], [22]. They could be different from those chosen by the authors in this work. For instance, available from published sources criteria for survivability outdoors, onset of fatality, and 15% of fatality probability are 21 kPa, 25 kPa, and 35 kPa respectively following UK's Health and Safety Executive [21]. All three values are below 100 kPa ("1% probability of fatality due to lung haemorrhage") selected here for the ***"fatality"*** deterministic separation distance.

The authors don't assumes any responsibility for the choice of harm criteria and assessment of deterministic separation distances further in this study. Instead, the methodology allows users to make their own choice of harm criteria. A user could select different harm criteria depending on scenarios chosen for carrying out the hydrogen safety engineering analysis [23]. It should be underlined that any demolition of a civil structure holds the threat to life. This should be accounted for during the safety design of hydrogen system or infrastructure.

8.2 Destructive pressure effects on civil structures

Figure 14 (left) shows three general thresholds (solid lines) for damage to buildings by a blast wave in the coordinates overpressure, ΔP, and impulse, I. "The basis for these curves is British data from enemy bombing in World War II plus records of explosions dating from 1871. Although this relationship was developed for the average British dwelling house, it also works fine for factories, main offices, and main engineering workshops" [10]. The levels of demolition effects to buildings are as follows (Figure 14, left). The *minor damage* involves the breakage of glass, wrenching of joints

occur and the removing of partitions out of fittings. The *major damage* involves the partial or total damage of the roof, partial damage of an external wall (at least one) and destruction of the load bearing partitions/members. The *partial demolition* involves the destruction or remaining unsafe of 50-75% of external brickwork/walls [10], [19]. It is important to stress that the area below the "Threshold for minor structural damage" curve is not free from building damage. Cormie et al. [24] state that this area refers to damage calling for urgent repair but is not severe enough to make the building uninhabitable: there would be damage to ceiling and tiling and more than 10% of glazing would be broken.

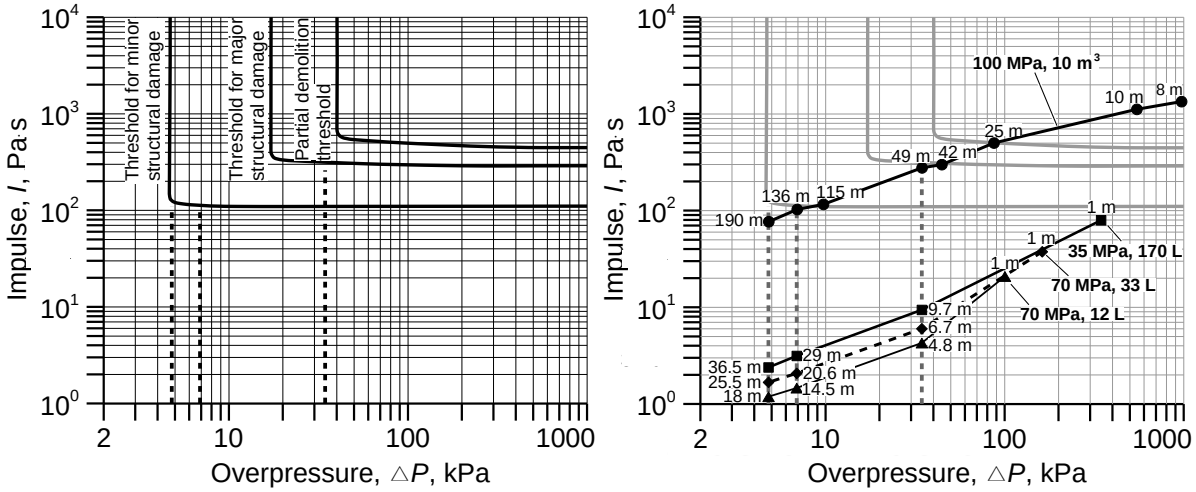

Figure 14. Left: overpressure-impulse thresholds for damage to buildings [10] (solid curves), and three overpressure thresholds from [20] (dash lines). Right: pathway (symbols are labelled by meters from the tank) of a blast wave from a tank rupture in a fire for four selected applications.

The minor structural damage of a building, following the thresholds suggested by Baker et al. [10], can be produced by a blast wave with overpressure in the range of 4.8-17.0 kPa and impulse above 130 Pa·s, as well as for any overpressure above 4.8 kPa if the impulse is in the range 130-300 Pa·s (see Figure 14, left). This curve is marked "Threshold for minor structural damage". The major structural damage is produced by overpressure in a blast wave varying in a range 17-40 kPa and the impulse above 340 Pa·s, and also at overpressure above 40 kPa and impulse of about 290-450 Pa·s. This curve is marked as "Threshold for major structural damage" in Figure 14 (left). The partial demolition requires overpressure above 40 kPa and impulse above 450 Pa·s. This curve is marked as "Partial demolition threshold".

However, the threshold curves from Baker et al. [10] give a limited assessment of a blast wave damage effect because they are built on the high explosives data only. Table 7 presents more data on damaging overpressures for buildings and structures. They can be used for further in-depth assessment of a blast wave impact. The selected thresholds for building damage from a blast wave overpressure applied further in this work are [20]: 4.8 kPa for ***minor damage***, 6.9 kPa for ***partial demolition***, and 34.5 kPa for ***almost total destruction***. These three criteria are shown in Figure 14 (left) by vertical black dash lines and in Figure 14 (right) by vertical grey dash lines.

Table 7. Pressure effects on buildings.

Element	Damage	Overpressure, kPa
Window frame	5% broken [20]	0.69-1.0
	50% broken [20]	1.45-2.5
	90% broken [20]	3.7-6.0
House	Minor damage to house structures [20]*	4.8
	Failure of doors and window frames [20]	5.3-8.9
	Partial demolition of house, turns unhabitable [20]**	6.9
	Partial collapse of walls and roof of house [20]	13.8
	50% destruction of brickwork of house [20]	17.3
	Almost total destruction of house [20]***	**34.5**-48.3
Other	Possible total destruction of building [20]	69
Industrial building	Break of cladding of light industrial building [20]	27.6
Heavy steel frame industrial building, single level, low strength wall [25]	Blowing-in of windows and doors, ripping off of light siding	7
	Distortion of frame (minor to major)	49.2
	Severe distortion/collapse of the frame	61.5
Reinforced concrete frame office building, 3-10 levels, low strength walls [25]	Blowing-in of doors and windows, ripping of light siding, cracking of interior partitions	7
	Moderate distortion of the frame, blow-down of interior partitions, spalling of concrete	55.4-61.5
	Severe distortion of the frame, incipient collapse	68.8-76

Notes: * - "***minor damage"*** threshold; ** - "***partial demolition"*** threshold; *** - "***almost total destruction"*** threshold.

9.0 BLAST WAVE EFFECTS AND SEPARATION FROM FOUR TYPICAL HYDROGEN APPLICATIONS

The developed model and methodology of a blast wave decay accounting for combustion of hydrogen released into the air is applied here to calculate the pressure effects and to estimate the corresponding harm to people and damage to buildings in accidents with four typical high-pressure hydrogen storage tanks. Both scenarios with stand-alone and under-vehicle hydrogen storage tanks rupture in a fire are considered.

The first application is a tank of 10 m^3 volume and storage pressure of 100 MPa at refuelling station [26] (line with circles in Figure 13 (right) and Figure 14 (right). The second application is the fuel cell vehicle on-board tank of 170 *L* and 35 MPa (line with squares). The third is an assumed imaginary vehicle with three tanks each 33 *L* and 70 MPa, which together are containing the same amount of hydrogen as in the previous vehicle application (dash line with diamonds). Only a blast wave from a rupture of one of three tanks in a fire will be considered here as a more probable event. The last, fourth, application is a scooter with a storage tank of 12 *L* volume and pressure of 70 MPa (line with triangles).

Figure 13 (right) shows by black lines (three solid lines and one dash line) blast wave pathways for all four applications in the coordinates overpressure-impulse to estimate deterministic separation distances for humans. Labels on the graph indicate the distance of the blast wave from the tank in meters. Figure 14 (right) shows the pathways for the blast wave in the coordinates impulse-overpressure to estimate the deterministic separation distances based on the selected in this paper damage criteria for buildings (different criteria can be selected by a user based on a type of building, see Table 7).

Table 8 shows the following parameters calculated for four selected applications: the dimensionless starting shock, $\bar{P}_{st}$, that can be easily transformed into dimensional starting shock by multiplication by the surrounding pressure; the dimensionless spherical vessel radius, $\bar{r}_v$, (used together with $\bar{P}_{st}$ to select a corresponding curve in Figure 5, left, and applied to four chosen applications in Figure 15 below); the dimensional radius of a spherical vessel of equivalent volume, r_v (blast wave cannot be calculated at distances from a vessel less than r_v); and the radius of hemisphere occupied by combustion products of burnt stoichiometric hydrogen-air mixture, r_b.

Table 8. Parameters $\bar{P}_{st}$, $\bar{r}_v$, r_v, and r_b of four selected hydrogen storage tank applications.

Application	Stand-alone: 10 m^3, 100 MPa	On-board: 170 *L*, 35 MPa	On-board: 33 *L*, 70 MPa	On-board: 12 *L*, 70 MPa
$\bar{P}_{st}$ (-)	110	54	80	80
$\bar{r}_v$ (-)	0.054	0.069	0.058	0.058
r_v (m)	1.34	0.34	0.2	0.14
r_b (m)	39.6	7.91	5.46	3.89

9.1 Refuelling station tank rupture in a fire (10 m^3 and 100 MPa)

Let us assess the consequences for humans and civil structures from the rupture of a stand-alone high-pressure hydrogen storage vessel of 10 m^3 volume with internal pressure of 100 MPa that can be hosted at refuelling stations [26]. Rupture of such storage vessel in a fire would release a huge amount of mechanical and chemical energy.

Overpressure and impulse in the blast wave are calculated, using the original methodology developed in this study and described in detail in previous sections, as follows. Firstly, the dimensionless starting shock overpressure, $\bar{P}_{st}$, is found using Figure 4 in section 4.0, or equations (12)-(13). For this, the speed of sound in high-pressure hydrogen and air are calculated using the corresponding equations in section 4.0, and their squared ratio is calculated as $(2121.04/343.2)^2=38.2$. The ratio of pressures is 987. Then, the dimensionless starting shock can be found as $\bar{P}_{st}=110$ (see Table 8).

Next step is to find the dimensionless radius of the vessel, which is calculated as $\bar{r}_v=r_v(p_s/E_m)^{1/3}$, where $r_v=(3V/4\pi)^{1/3}$, and $E_m=[(p_g-p_s)(V-mb)]/(\gamma-1)$ (see section 4.0). In this case the equivalent by volume spherical vessel radius and the stored mechanical energy are respectively: $r_v=(3\cdot 10\ m^3/4\cdot 3.14)^{1/3}=1.34$ m, and $E_m=[(1\times10^8\ Pa - 1.01\times10^5\ Pa)(10\ m^3 - 505.5\ kg\cdot 7.69\times10^{-3}\ m^3/kg)]/(1.39-1)=1.566\times10^9$ J. The mass of hydrogen (505.5 kg) was calculated using the Abel-Noble equation for real gas. Then, the dimensionless radius of the spherical vessel is $\bar{r}_v=r_v(p_s/E_m)^{1/3}=1.34\cdot(1.01\times10^5\ Pa\ /\ 1.566\times10^9\ J)^{1/3}=0.054$.

Afterwards, the calculated values of dimensionless starting shock overpressure and dimensionless radius of the vessel are used to select one of the existing curves or to build a new curve in Figure 5 (left) for each of four chosen for analysis applications. The curve has to be plotted by paralleling it with an adjacent existing curve(s) shown in Figure 15 by grey lines.

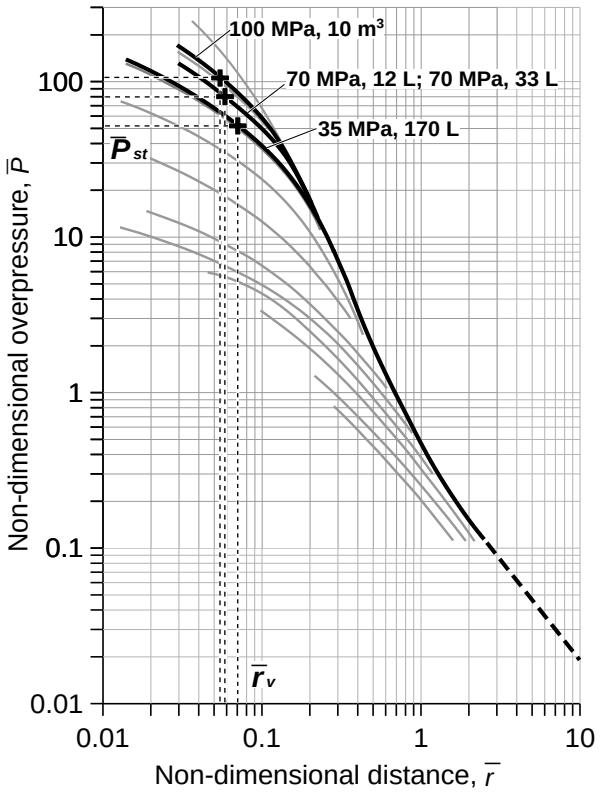

Figure 15. New curves build for four selected applications in the coordinates dimensionless distance-overpressure using Baker et al. curves [10]. Crosses - intersection of dash lines corresponding to calculated starting shock, $\bar{P}_{st}$, and vessel radius, $\bar{r}_v$, for each application.

The selected/new curves in Figure 5 (left), which are explicitly shown in Figure 15 by thick black solid lines, are used then to find out the dimensionless overpressure in a blast wave at particular dimensionless distances. It can be used as well to solve the inverse problem, i.e. to find out the dimensionless distance at which the particular dimensionless overpressure in a blast wave will be achieved. The dimensionless distance from a tank, $\bar{r}=\bar{r}_P$, is defined by equation (16). This equation is used to calculate a dimensional radius. The dimensional pressure can be easily calculated by multiplication of the dimensionless pressure by the surrounding pressure. For example, in this particular case of storage tank at refuelling station the dimensional overpressure in the starting shock is $\Delta P_{st}=110\cdot1.013\times10^5$ Pa=11.15 MPa. Even this overpressure is quite large, it is about 10 times less compared to the storage pressure.

For estimation of a dimensional impulse the following two steps should be undertaken following the developed methodology. Firstly, a dimensionless distance, $\bar{r}_I$, in Figure 5 (right) has to be applied to find out a corresponding value of a dimensionless impulse, $\bar{I}$. The dimensionless distance is calculated as $\bar{r}_I=r[p_s/\alpha\cdot E_m]^{1/3}$, by substitution of the dimensional radius, r, into this equation. Secondly, the determined dimensionless impulse is used to calculate the dimensional impulse by the equation: $I=\bar{I}$ $[p_s^{2/3}(\alpha\cdot E_m)^{1/3}]/a_s$.

Table 9 gives the deterministic separation distances for four typical hydrogen applications calculated by the developed technique with criteria for harm to people and damage to building defined in the previous section. It has to be underlined that a user could choose different harm and damage criteria, which surely will affect the values of the deterministic separation distances.

Table 9. Deterministic separation distances for humans and buildings for four selected typical hydrogen storage applications.

Object	Criterion for separation	Deterministic separation distance, m			
		Stand-alone:	On-board:		
		10 m^3, 100 MPa	170 *L*, 35 MPa	33 *L*, 70 MPa	12 *L*, 70 MPa
Humans	No-harm [10]	470	90	57	35
	Injury [20]	78	16	11	7.5
	Fatality [20]	23	2	1.4	1
Buildings [17]	Minor damage [20]	190	36.5	25.5	18
	Partial demolition [20]	136	29	20.6	14.5
	Almost total destruction [20]	49	9.7	6.7	4.8
Buildings [8]	Minor damage [10]	115	-	-	-
	Major damage [10]	42	-	-	-
	Partial demolition [10]	25	-	-	-

In the case of 10 m^3 and 100 MPa tank rupture in a fire at refuelling station the "no-harm" separation distance for people is as high as 470 m (see Figure 13, right). The "injury" separation distance is 78 m, and the deterministic "fatality" separation is 23 m. These are quite large distances and hydrogen safety engineering should be applied to prevent an accident as a mitigation of the consequences is questionable. It should be noted, that in this particular case r_b=39.6 m. Considering r_b as an indicator of the fireball size the actual "fatality" deterministic separation distance could be somewhat larger than 40 m (if to take into account the radiation from the fireball). The distance at which the "minor damage" [20] of the building shall occur is 190 m (without consideration of the thermal effects from the fireball). The "partial demolition" [20] of the buildings will be observed at 136 m. The "almost total destruction" [20] of houses will be within deterministic separation distance of 49 m.

The deterministic separation distances depend on the damage criteria selected by a user. Let us estimate the effect of the damage criteria choice on the separation distance using criteria from [17] and [8] for the case of stand-alone tank at refuelling station (see Table 9, and Figure 14, right). The application of damage criteria by Baker et al [10] gives the following deterministic separation distances: 115 m for the minor damage, 42 m for the major damage, and 25 m for the partial demolition. These distances are shorter compared to distances calculated by similar criteria taken from Mannan [17]. Authors have chosen to use criteria by Mannan [17] due to the fact that the application of the criteria by Baker et al [10] would not give even a minor damage for three onboard tank applications considered here as examples (see Figure 14, right). The last seems to be unrealistic for overpressures of about 0.35 MPa.

These large separation distances clearly indicate the necessity of thermal protection of such tanks in the case of fire either external or related to hydrogen leak from this tank, e.g. when tank is located at least partially in an artificial shell like reinforced concrete pit at station grounds. Location of a tank at a roof of a refuelling station looks like a possible "mitigation" (coefficient α will be probably reduces from its 1.8 value due to deviation from the hemispherical symmetry). However, this type of design has to be validated experimentally.

9.2 Vehicle tank rupture in a fire (170 L, 35 MPa)

The deterministic separation distance for humans and buildings, that can be affected by the blast wave generated after the on-board tank (170 *L*, 35 MPa [27], [28]) rupture, when a vehicle has caught a fire, are shown in Table 9. This tank contains 4 kg of hydrogen (calculated using the Abel-Noble gas equation).

The "no-harm" separation distance for humans would be 90 m, the "injury" separation distance – 16 m, and the "fatality" separation – 2 m. Corresponding distances to building are: the "minor damage" distance is 36.5 m, the "partial demolition" – 29 m, and the "almost total destruction" – 9.7 m.

9.3 Vehicle tank rupture in a fire (33 L, 70 MPa)

Let us consider a hydrogen storage system comprising three tanks. The three tanks system shall store the same amount of hydrogen as in the previous example with one tank (170 *L*, 35 MPa, 4 kg of hydrogen). For instance, if the storage pressure in a tank is 70 MPa then the volume of each tank is 33 *L* (calculated by Abel-Noble real gas equation) to store altogether the same 4 kg of hydrogen. This is of interest to compare the safety strategies chosen by different OEMs for on-board hydrogen storage, i.e. to use one larger tank or three smaller tanks. We assume in our calculations that only one of three tanks fails.

The no-harm separation distance to human would be 57 m (37% less than 90 m produced by the larger volume 170 *L* but smaller pressure of 35 MPa tank rupture). The deterministic separation distance to buildings with the "minor damage" decreases from 36.5 m (for 170 *L* and 35 MPa) to 25.5 m (for 33 *L* and 70 MPa), i.e. by 39%. Thus, the smaller tank rupture gives the notably shorter deterministic separation distances. It may be considered as a possible safety strategy for reduction of the deterministic separation distances from a blast wave.

9.4 Vehicle tank rupture in a fire (12 L, 70 MPa)

Another example is an on-board hydrogen tank installed on a scooter [29], [30] that has a capacity of 12 *L* and storage pressure of 70 MPa. For such tank rupture in a fire the "no-harm" separation distance can be estimated as 35 m, the "injury" distance as 7.5 m, and the "fatality" deterministic separation distance as 1 m. The damage to buildings separation distances are: the "minor damage" is 18 m, the "partial demolition" is 14.5 m, and the "almost total destruction" is 4.8 m.

10.0 CONCLUSIONS

The original methodology for calculation of overpressure and impulse in a blast wave from a high-pressure gas storage tank rupture in a fire is developed. The methodology is built up using the novel model of combustion of hydrogen in air at the contact surface and behind it in the wake of the outward propagating shock. The Abel-Noble equation of state for real gas is applied to calculate parameters of hydrogen in a tank, including the amount of stored mechanical (internal) energy similar to the Brode's model. The dimensionless starting shock is calculated in the model using the speed of sound in the real gas. The use of the ideal gas equation of state in the former models significantly overestimates the mechanical energy of the compressed gas, e.g. by 64% for hydrogen storage pressure of 100 MPa.

The former techniques without combustion are unable to reproduce blast wave decay in the experiments with high-pressure hydrogen tanks rupture in the fire. This is especially related to the under-vehicle test conditions. The predictions by the methodology's compared against experimental data on the blast waves obtained during tests performed in the USA with a stand-alone and an under-vehicle high-pressure hydrogen storage tank rupture in the bonfire test. The significance of this study is in the methodology capability to predict more accurately the experimentally measured maximum overpressures and impulses at different distances. The developed model with combustion is even able to reproduce the experimentally observed "plateau" in a blast wave overpressure as a function of distance in the under-vehicle test, thus demonstrating its rigour.

The inverse problem method is applied to determine the mechanical energy coefficient, α, and the chemical energy coefficient, β, in two typical configurations. For the stand-alone high-pressure hydrogen storage tank, it is found that α=1.8 (accounts for the ground cratering effect in the hemispherical geometry of a blast wave) and β=0.052; for the under-vehicle tank the coefficients are α=0.12 and β=0.09. The decrease in the mechanical energy coefficient, α, can be explained by losses of internal energy of compressed gas to deform and dislocate the vehicle from its original location by

22 m in the test. The increase in chemical energy coefficient β is thought to be due to the vehicle obstruction facilitating the turbulent combustion, and the weaker shock that gives more time for combustion to contribute to the blast wave strength in the under-vehicle tank test.

The fraction of the stored combustion energy released during the stand-alone tank fire test and fed into the blast wave is determined by the inverse problem method as about 5% (β=0.052). For the under-vehicle tank test this fraction is increased by about twice to 9% (β=0.09). In spite of this comparatively small fraction of combustion energy released during the shock propagation, it has been found that the fraction of chemical energy feeding the blast wave is larger than even the total amount of stored mechanical energy of the compressed gas. The ratio of chemical to mechanical energies released to feed the blast wave is 1.4 for the stand-alone tank test, and 30 (!) for the under-vehicle tank test.

The performed parametric study demonstrated that accounting for the drift of initial pressure and temperature of hydrogen before the rupture due to heat transfer from the fire into the tank gives an error about 5% for the considered tests. The use of a fireball diameter observed in experiments proved not to be a choice for the methodology due to the uncontrolled effects of various parameters on the measured fireball size, and the absence of corresponding reliable and validated predictive models, if possible for hydrogen at all.

The developed methodology has been applied to analyse the potential consequences of the rupture of four typical high-pressure hydrogen storage tanks in a fire using the selected by the authors harm criteria for people and the damage criteria for buildings from blast waves published elsewhere. Typical hydrogen applications include a refuelling storage tank, two fuel cell vehicle on-board storage tanks, and a tank on a scooter. It should be underlined, that the harm and damage criteria selected by the authors in this study are for demonstration purposes only. Hydrogen safety engineers and other responsible for safety professionals have to choose the criteria following international and/or national regulations.

The importance of the exclusion of a fire in the vicinity of a stationary storage tank at refuelling station as much as possible, and the thermal protection of an on-board tank to prevent its rupture in a fire are demonstrated and underlined. The methodology can be used for development of safety strategies for high-pressure hydrogen storage systems, e.g. for the choice of a number of storage tanks accommodating the same amount of hydrogen in a vehicle.

This study has addressed one of the knowledge gaps in hydrogen safety science and engineering, i.e. the development of a predictive model of a blast wave decay for assessment of deterministic separation distances in the case of storage tank rupture in a fire. The model is recommended for use as a tool for hydrogen safety engineering. More bonfire tests with a rupture of a stand-alone and an under-vehicle tanks of different volume at different storage pressures are needed to expand the validation domain of the model and to enrich the knowledge about consequences of catastrophic failure of a hydrogen storage tank in a fire. The methodology can be used for safety engineering design of systems and infrastructure with other compressed gases after the calibration of empirical coefficients α and β against appropriate experimental data.

11.0 ACKNOWLEDGEMENTS

The authors are grateful to the Fuel Cell and Hydrogen Joint Undertaking for funding this work through the HyResponse project (www.hyresponse.eu), grant agreement No.325348; and the Engineering and Physical Sciences Research Council (UK) for funding the study through The Hydrogen and Fuel Cells Supergen Hub project (http://h2fcsupergen.com/), grant number EP/J016454/1. They would like to thank also Dr Simon Jallais for his valuable comments.

REFERENCES

[1] V. Molkov, *Fundamentals of Hydrogen Safety Engineering*. bookboon.com, 2012.

[2] V. V. Molkov and J.-B. Saffers, "Hydrogen jet flames," *International Journal of Hydrogen Energy*, vol. 38, no. 19, pp. 8141–8158, Jun. 2013.

[3] P. Waite, "Relative frequency of failure modes," 2012. [Online]. Available: http://h2safe.com/case_safety.html. [Accessed: 11-Apr-2014].

[4] R. Zalosh, "Blast waves and fireballs generated by hydrogen fuel tank rupture during fire exposure," in *5th International Seminar on Fire and Explosion Hazards*, Edinburgh, UK, 2007.

[5] D. A. Crowl, *Understading explosions*. American institute of chemical explosions, 2003.

[6] H. L. Brode, "Blast Waves from a Spherical Charge," in *Physics of Fluids*, 1959, vol. 2, pp. 217–229.

[7] J. M. Smith and H. C. Van Ness, *introduction to Chemical Engineering Thermodynamics*, 4th ed. New York: McGraw-Hill, 1987.

[8] D. A. Crowl, "Calculating the energy of explosion using thermodynamic availability," *J.Loss prev. Process Ind.*, vol. 5(2), pp. 109–118, 1992.

[9] L. D. Landau and E. M. Lifschitz, *Fluid dynamics*, 3rd ed., vol. 6. Moscow, 1986.

[10] W. E. Baker, P. A. Cox, P. S. Westine, J. J. Kulesz, and R. A. Strehlow, *Explosion hazards and evaluation*. Elsevier Scientific Publishing Company, 1983.

[11] V. I. Krutov, S. I. Isaev, I. A. Kozhinov, N. P. Kozlov, V. I. Kofanov, B. M. Mironov, V. M. Nikitin, G. B. Petrazhitskiy, A. M. Pylaev, B. I. Khvostov, and E. B. Shishov, *Technical Thermodynamics*, vol. 3. Moscow, 1991.

[12] I. Johnson, "The Noble-Abel Equation of State: Thermodynamic Derivations for Ballistics Modelling," Weapons Systems Division, Defence Science and Technology Organisation, DSTO-TN-0670, 2005.

[13] N. Weyandt, "Analysis of Induced Catastrophic Failure Of A 5000 psig Type IV Hydrogen Cylinder," Southwest Research Institute report for the Motor Vehicle Fire Research Institute, 01.06939.01.001, 2005.

[14] N. Weyandt, "Vehicle bonfire to induce catastrophic failure of a 5000-psig hydrogen cylinder installed on a typical SUV," Southwest Research Institute report for the Motor Vehicle Fire Research Institute, 2006.

[15] R. Zalosh and N. Weyandt, "Hydrogen fuel tank fire exposure burst test," *SAE Pap.*, vol. 2005–01–1886, 2005.

[16] Ineris, Accident risks devision, "EAT-DRA-76-Formalization of knowledge and tools in the area of major risks. Vessel bursts, phenomenology and effect modelling-Omega 15," 2012.

[17] S. Matsuo, S. Koyama, J. Nagao, and T. Setoguchi, "Flow Characteristics of High-Pressure Hydrogen Gas in the Critical Nozzle," *OTEC*, pp. 53–57, 2009.

[18] M. V. Bragin, D. V. Makarov, and V. V. Molkov, "Pressure limit of hydrogen spontaneous ignition in a T-shaped channel," vol. 38, no. 19, pp. 8039–8052, Jun. 2013.

[19] W. E. Baker, J. J. Kulesz, R. E. Ricker, R. L. Bessey, P. S. Westine, V. B. Parr, and G. A. Oldham, "Workbook for predicting pressure wave and fragment effects of exploding propellant tanks and gas storage vessels," Technical Report NASA-CR-134906, 1975.

[20] S. Mannan, *Lees' Loss Prevention in the Process Industries*, 3rd ed., vol. 1. Elsevier Butterworth-Heinemann, 2005.

[21] Health and safety executive, "Indicative human vulnerability to the hazardous agents present offshore for application in risk assessment of major accidents," *SPC/Tech/OSD/30*, 2006.

[22] T. F. Barry, *Risk-Informed, Performance-Based Industrial Fire Protection*, 1st ed. USA: Tennessee Valley Publishing, 2002.

[23] J.-B. Saffers and V. Molkov, "Hydrogen safety engineering framework and elementary design safety tools," *Int. J. Hydrog. Energy*, vol. 39, no. 11, pp. 6268–6285, 2014.

[24] D. Cormie, G. Mays, and P. Smith, *Blast effects on buildings*, 2nd ed. Thomas Telford Limited, 2009.

[25] R. M. Jeffries, S. J. Hunt, and L. Gould, "Derivation of fatality probability function for occupants buildings subject to blast loads," WS Atkins Science & Technology, Contract research report for HSE 147/1997, 1997.

[26] P. S. Heggem, “Safe and Efficient Energy Storage,” in *Presentation for EPSRC project kick-off meeting: “Integrated safety strategies for onboard H2 storage,”* University of Ulster, 2013.
[27] “Honda FCX Clarity,” 2015. [Online]. Available: http://en.wikipedia.org/wiki/Honda_FCX_Clarity. [Accessed: 02-Jun-2015].
[28] “FCX Clarity,” 2015. [Online]. Available: http://automobiles.honda.com/fcx-clarity/specifications.aspx. [Accessed: 02-Jun-2015].
[29] Intelligent Energy, “Zero Emission Fuel Cell Scooter,” 2014. [Online]. Available: http://www.intelligent-energy.com/automotive/case-studies/suzuki. [Accessed: 13-Oct-2014].
[30] K. Ash, “Suzuki Fuel Cell Burgman,” 2014. [Online]. Available: http://www.ashonbikes.com/content/suzuki-fuel-cell-burgman. [Accessed: 13-Oct-2014].